Applied Thermal Engineering

Forecasting green roofs' potential in improving building thermal performance and mitigating urban heat island in the Mediterranean area: an artificial intelligence-based approach

--Manuscript Draft--

Manuscript Number:	
Article Type:	Original Research Article
Keywords:	Green roof; Thermal performance; Urban heat Island; Mediterranean area; Artificial Intelligence
Corresponding Author:	Domenico Mazzeo, PhD University of Calabria Rende, Cosenza ITALY
First Author:	Domenico Mazzeo, PhD
Order of Authors:	Domenico Mazzeo, PhD
	Nicoletta Matera, PhD
	Giorgia Peri, PhD
	Gianluca Scaccianoce, PhD
Abstract:	Green roofs are widely used in hot or cold climates mainly because they are capable to improve the energy efficiency of buildings and, when implemented at a large scale, reducing air pollution and the urban heat island effect (UHI) in urban contexts. However, the study of green roof thermal performance is a challenge because of both the occurrence of different mass and thermal exchange phenomena contemporaneously present (convective, shortwave and longwave radiative heat exchanges between the outdoor environment and substrate and vegetation, evapotranspiration, heat conduction through the substrate and so on) and the non-linearity of existing mathematical models describing these phenomena. Artificial Neural Network (ANN) black-box algorithms, which are increasingly being used to perform predictive analyses in various fields of engineering science, among which the building sector, are a valid alternative to studying such complex systems. However, the literature highlights that to date limited attention has been paid to such a research topic and that the few available studies are concentrated on specific individual aspects of the green roofs' performance, such as evapotranspiration or irrigation management; no research is yet available that couples the ANN concept to the evaluation of all the main thermal parameters that intervene in its thermal performance. In addition, - quite surprisingly – none of the available research refers to coupling ANNs and green roofs in the Mediterranean area, where green roofs are instead considered one of the most suitable technologies to reduce the high cooling demand. Therefore, the objective of this research work is to create and validate an ANN for the prediction of the monthly green roof's internal and external surface temperatures and the monthly internal air temperature, starting from different green roof parameters and climatic variables. Specifically, the ANN was created with reference to a Mediterranean climate considering an existing green roof on a building of the University of Palermo characterized by a cooling demand predominance; 180 green roof configurations, obtained by varying the characteristic parameters of vegetation (plant height, leaf area index and leaf reflectivity) and the substrate thickness and thermophysical properties (lightweight and heavyweight), were dynamically simulated on an hourly basis to build the training dataset. In addition, other 72 green roof configurations were simulated to generate the dataset for the validation purpose of the ANN accuracy. Moreover, the optimal number of neurons and hidden layers was investigated. The optimal ANN-related architecture consists of 90 neurons with one hidden layer and guarantees very high accuracy predictions. The outcomes of this research represent a useful tool to determine the thermal response of green roofs and so their impact on the energy demand of buildings equipped with them, the indoor thermal comfort, and the UHI phenomenon.

Suggested Reviewers:	Mohammad Saffari, PhD Postdoc researcher fellow, Dublin City University mohammad.saffari@dcu.ie He is an expert in this sector
	Karolos J. Kontoleon, PhD Associate professor, Aristotle University of Thessaloniki kontoleon@civil.auth.gr He is an expert in this field

Dear **Editor-in-Chief**
Professors Christos N. Markides

I'm writing to communicate that our article has been uploaded on 27th June 2022 on the Elsevier Editorial System for the *Applied Thermal Engineering* Journal.

Title of the article: Forecasting green roofs' potential in improving building thermal performance and mitigating urban heat island in the Mediterranean area: an artificial intelligence-based approach

Authors: Domenico Mazzeo[1,*], Nicoletta Matera[2], Giorgia Peri[3], Gianluca Scaccianoce[3]

[1]Department of Mechanical, Energy and Management Engineering (DIMEG), University of Calabria, Rende (CS), 87036, Italy
[2]Indipendent researcher, Rende (CS), 87036, Italy
[3]Department of Engineering, University of Palermo, Palermo, 90128, Italy

Research context and gap

The use of this green roofing technology is becoming more and more widespread, as it is a valid strategy to minimize the problems resulting from urban overbuilding because it provides several advantages both from an environmental, social, and economic perspective, as well as to the building on which they are installed.

To describe the thermal behaviour of a green roof, a variety of mathematical models have been proposed in the literature, which however have been validated only for specific green roof configurations and locations. Obviously, it is inaccurate to define one model as more or less appropriate than another, and it is also not possible to define the most appropriate model to use, because all models start from simplified assumptions, and some consider factors in detail, while others are neglected or ignored.

Among the available green roof models, the one proposed by Sailor in 2008 [18], which is based on the energy and mass balance equations of FASST [19], is certainly worth mentioning; it analyzes in detail each type of heat exchange occurring in the system of soil - vegetation - external environment, even if a simplified representation of the water balance and a constant soil thermal conductivity are proposed. This model was then implemented in the simulation program Energy Plus and validated with experimental data.

On the other hand, it should be noted that for the analysis of complex systems the use of artificial intelligence is increasingly being used in engineering science, as an alternative solution to perform predictive analyses in various fields.

A search in scientific databases has shown how there is still little use of this technique in the field of green roofs: only six research works have coupled the artificial intelligence model and green roof analysis.

The analysis of these few research works highlights that to date attention has been given to specific individual aspects influencing the green roof performance such as irrigation and the evapotranspiration phenomenon and to specific thermal quantities, with the surface temperature the most frequent. In addition, the cooling period is predominant as the season selected for their evaluation. However, except for the work of Erdemir et al. [33], ***no research is yet available that couples the ANN concept to the evaluation of all the main thermal parameters that intervene in the green roof performance.***

Research objectives

To cover this research gap, this work proposes an algorithm code based on ANNs able to predict the thermal performance of a green roof on the basis of monthly values of climatic variables. Specifically, the idea behind this study is to apply ANNs to learn the thermal response of a green roof deriving from the joint action of all different thermal forcings. In detail, the tool developed trained with monthly data is able to predict the monthly external and internal green roof surface temperatures and internal air temperatures.

All these quantities are also strictly correlated to the UHI, the indoor thermal comfort, and cooling load transferred indoors. Consequently, the tool proposed here can also contribute to assessing the impact that green roofs have on these phenomena and aspects.

To achieve the purpose of the study, different green roofs were considered located in the city of Palermo, characterized by a Mediterranean climate, by varying the most important vegetation and soil parameters. The ANN was trained and validated on the basis of monthly data of external climatic conditions and other monthly green roof thermal performance indicators. The monthly data derives from dynamic hourly simulations. Training and validation data derive from an extensive parametric analysis performed by the present authors using Design Builder Software.

Thank you for your consideration! Waiting to receive your reply soon

Your Sincerely, *Dr. Domenico Mazzeo*

University of Calabria, Department of Mechanical, Energy and Management Engineering (DIMEG),

*Corresponding author contact information:

Domenico Mazzeo, Post-doc Research fellow, email address: domenico.mazzeo@unical.it

Highlights

- A research gap related to a very limited coupling of AI and green roofs was identified
- A very accurate ANN able to estimate the thermal performance of green roofs was optimized
- 180 green roof configurations were dynamically simulated to train different ANNs
- ANN validation was performed considering other 72 green roof configurations
- Green roof impact on building thermal comfort and energy demand and UHI mitigation

Graphical Abstract

Green roof artificial neural network (ANN)

Step 1 - Database creation

Parametric analysis

Hourly simulations throughout the year

252 different green roofs

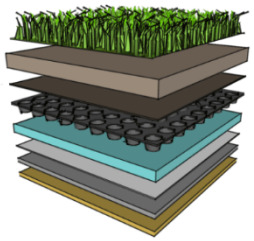

Step 2 - ANN training and optimization

ANN design

Number of neurons
Number of hidden layers

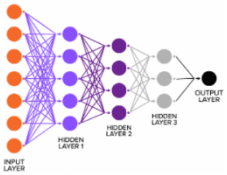

Training database: 180 different green roofs

Inputs and outputs

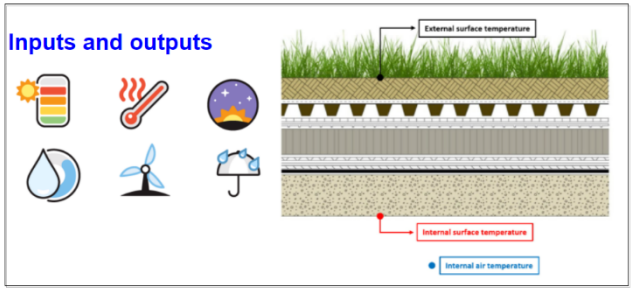

Step 3 - ANN validation

ANN accuracy
ANN validation

Validation database: 72 different green roofs

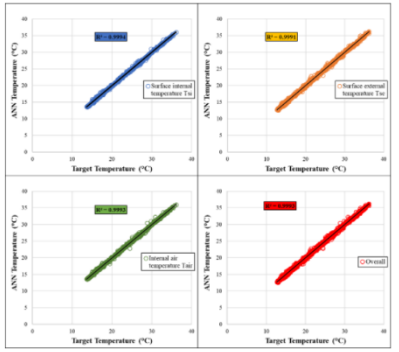

Forecasting green roofs' potential in improving building thermal performance and mitigating urban heat island in the Mediterranean area: an artificial intelligence-based approach

Domenico Mazzeo[1,*], Nicoletta Matera[2], Giorgia Peri[3], Gianluca Scaccianoce[3]

[1]Department of Mechanical, Energy and Management Engineering (DIMEG), University of Calabria, Rende (CS), 87036, Italy
[2]Independent Researcher, Rende (CS), 87036, Italy
[3]Department of Engineering, University of Palermo, Palermo, 90128, Italy

*Corresponding author: domenico.mazzeo@unical.it

Highlights

- A research gap related to a very limited coupling of AI and green roofs was identified
- A very accurate ANN able to estimate the thermal performance of green roofs was optimized
- 180 green roof configurations were dynamically simulated to train different ANNs
- ANN validation was performed considering other 72 green roof configurations
- Green roof impact on building thermal comfort and energy demand and UHI mitigation

Abstract

Green roofs are widely used in hot or cold climates mainly because they are capable to improve the energy efficiency of buildings and, when implemented at a large scale, reducing air pollution and the urban heat island effect (UHI) in urban contexts.

However, the study of green roof thermal performance is a challenge because of both the occurrence of different mass and thermal exchange phenomena contemporaneously present (convective, shortwave and longwave radiative heat exchanges between the outdoor environment and substrate and vegetation, evapotranspiration, heat conduction through the substrate and so on) and the non-linearity of existing mathematical models describing these phenomena.

Artificial Neural Network (ANN) black-box algorithms, which are increasingly being used to perform predictive analyses in various fields of engineering science, among which the building sector, are a valid alternative to studying such complex systems. However, the literature highlights that to date limited attention has been paid to such a research topic and that the few available studies are concentrated on specific individual aspects of the green roofs' performance, such as evapotranspiration or irrigation management; no research is yet available that couples the ANN concept to the evaluation of all the main thermal parameters that intervene in its thermal performance. In addition, - quite surprisingly – none of the available research refers to coupling ANNs and green roofs in the Mediterranean area, where green roofs are instead considered one of the most suitable technologies to reduce the high cooling demand.

Therefore, the objective of this research work is to create and validate an ANN for the prediction of the monthly green roof's internal and external surface temperatures and the monthly internal air temperature, starting from different green roof parameters and climatic variables. Specifically, the ANN was created with reference to a Mediterranean climate considering an existing green roof on a

building of the University of Palermo characterized by a cooling demand predominance; 180 green roof configurations, obtained by varying the characteristic parameters of vegetation (plant height, leaf area index and leaf reflectivity) and the substrate thickness and thermophysical properties (lightweight and heavyweight), were dynamically simulated on an hourly basis to build the training dataset. In addition, other 72 green roof configurations were simulated to generate the dataset for the validation purpose of the ANN accuracy. Moreover, the optimal number of neurons and hidden layers was investigated. The optimal ANN-related architecture consists of 90 neurons with one hidden layer and guarantees very high accuracy predictions.
The outcomes of this research represent a useful tool to determine the thermal response of green roofs and so their impact on the energy demand of buildings equipped with them, the indoor thermal comfort, and the UHI phenomenon.

Keywords: Green roof; Thermal performance; Urban heat Island; Mediterranean area; Artificial Intelligence.

1. Introduction

Background

Roofs with greenery growing on top are called green roofs. The use of this green roofing technology is becoming more and more widespread, as it is a valid strategy to minimize the problems resulting from urban overbuilding because it provides several advantages both from an environmental, social, and economic perspective, as well as to the building on which they are installed [1]. In detail, green roofs contribute to lowering noise levels [1-4] as well as reducing water runoff by minimizing the impact on sewer systems, as well as improving the quality of water runoff with reduced dust, pollutants, and nutrients [1, 5]. The purpose of green roofs is to counter high levels of atmospheric pollution by acting as vegetation that can intercept pollutants (PM10 particulate matter and PM2.5 particulate matter) as well as absorb carbon dioxide (CO_2), creating oxygen (O_2), and subsequently develop their vital functions [1, 6]. Moreover, they improve the efficiency of photovoltaic systems [7-9]. As for the energy advantages, this innovative solution can increase the cooling capacity, the shading effect, the surface albedo, when compared with, for example, an asphalt surface, and improve the thermal insulation of the building by decreasing the air conditioning load, especially during the summer months and therefore the corresponding greenhouse gas emissions [1, 10-12]. Plants growing on these roofs, whether extensive or intensive, are meant to absorb the incident radiation from the sun in order to perform their biological functions such as photosynthesis, transpiration, evaporation and respiration. In addition, evapotranspiration is useful for regulating the microclimate because it cools both the foliage and the surrounding air. In this way, these innovative solutions can limit the rise in ambient temperature on days where there is high solar radiation, thus mitigating the Urban Heat Island (UHI) effect [13]. In this regard, it is worth noting that the Mediterranean climate is one of the warmest climates worldwide in the summer period and the cooling demand in this season is often predominant in the energy demand. Consequently, green roofs for these areas can be selected as a promising solution both to reduce energy needs and UHI effects. Green roof covers can also attenuate and delay the temperature and heat flux acting on their surface given the high thermal mass of the substrate layer [14].

An average green roof installation cost of 99 €/m^2 is associated with extensive installations, 130 €/m^2 is associated with semi-intensive installations and 362 €/m^2 with those that host heavier materials and plants (i.e., small trees) [1].
Numerous studies in the literature suggest that from an energy standpoint, the use of green roofs is an excellent strategy for reducing heat transfers between a building's interior and exterior as well as improving thermal comfort within the building [15, 16]. Benefits are influenced by the characteristics of the system (leaf area, substrate type, depth and moisture content, materials of each layer and connection to the building), the physical characteristics of the building (geometry, height, insulation, building materials, building envelope, glazed area, solar orientation, shading) and local climatic conditions (seasons, heating or cooling needs) [1, 7, 17].
From a thermophysical perspective, the green roof system as a whole can be described by an energy balance equation that explains in a very general way the processes that are clarified in more depth and with different levels of detail in the following terms:

$$R_n = L + Q_{sens} + Q_{cond} + B \quad (1)$$

R_n is the radiative contribution which is composed of a short wave portion coming from the sun and a long wave portion. Most of the radiant energy that reaches the earth's surface is shortwave, a percentage of which is reflected by the surfaces on which it impinges. The percentage fraction of energy reflected, referred to as the albedo, depends on both time-varying environmental factors, such as the height of the Sun above the horizon, and the characteristics of the surface reached by the sun's rays. Vegetation usually reflects a higher fraction of radiation than soil. Part of the radiative energy absorbed by the earth is radiated back to the atmosphere in the longwave field, infrared, in a manner proportional to surface temperature. The same happens for the gases that constitute the atmosphere, which in turn reflect this energy in the same length field. Therefore, the net radiation, considered for the budget, turns out to be a combination of longwave and shortwave radiation. Ultimately, the detectable radiative contributions in the presence of a green roof are: short-wave radiation incident on foliage, short-wave radiation incident on the ground, longwave radiation between vegetation and the outdoor environment, longwave radiation between vegetation and soil, longwave radiation between soil and external environment.
L is the latent heat, transmitted by variation of liquid-vapour state; it is related to evapotranspiration phenomena, that is to say, soil evaporation and plant transpiration; the contribution of latent heat that propagates inside the soil should not be neglected, even if less important than the previous one. In latent processes the presence of water is fundamental; its absence tends to cancel the latent contribution leading to the transformation of the incident radiative contribution in part in sensible heat and part in conductive flow inside the soil.
Q_{sens} is the sensible heat flux, *i.e.*, the heat exchanged between the soil and the layer of air in contact, or between the vegetation and the surrounding air, due to a thermal gradient that generates air motions and thus heat propagation in the boundary layer by natural convection.
Q_{cond} is the heat flux in the soil, or the heat transferred from the surface to the underlying layers always triggered by a temperature gradient and dependent on the thermal conductivity of the layer that is being analyzed. This term can assume positive or negative values depending on whether there is heating or cooling of the surface. The thermal conductivity is closely related to the conditions of

humidity of the soil, as the air, a bad conductor of heat, present in the pores, can then be replaced by water, which instead is a good conductor.
B is the energy released into the biosphere by the photosynthesis process of plants, which, using the energy derived from sunlight, water and CO_2, release O_2 and produce biomass. This contribution is generally overlooked.
In consideration of all this, it can be deduced how complex the physical-thermal modelling of a green roof is. To describe the thermal behaviour of a green roof, a variety of mathematical models have been proposed in the literature, which however has been validated only for specific green roof configurations and locations. Obviously, it is inaccurate to define one model as more or less appropriate than another, and it is also not possible to define the most appropriate model to use, because all models start from simplified assumptions, and some consider factors in detail, while others are neglected or ignored. However, it should be noted that some models are supported by a process of validation that demonstrates the agreement between the theoretical mathematical model and the results obtained by experimental investigation.
Among the available green roof models, the one proposed by Sailor in 2008 [18], which is based on the energy and mass balance equations of FASST [19], is certainly worth mentioning; it analyzes in detail each type of heat exchange occurring in the system of soil - vegetation - external environment, even if a simplified representation of the water balance and a constant soil thermal conductivity are proposed. This model was then implemented in the simulation program Energy Plus and validated with experimental data.
On the other hand, it should be noted that for the analysis of complex systems the use of artificial intelligence is increasingly being used in engineering science, as an alternative solution to perform predictive analyses in various fields. Artificial intelligence, through artificial neural networks (ANNs), has been used, *e.g.*, for the assessment of energy and environmental performance of buildings [20], for the rehabilitation of non-residential building stock [21], as well as for the assessment of thermal transmittance in walls [22]. ANNs are also used as a valid and effective solution to provide predictive analysis of solar radiation [23], including monthly average [24] and daily average [25], wind energy [26, 27], as well as the maximum and normal operating power of a photovoltaic module [28]. Recently, ANNs were also employed to study the energy performance of clean energy communities based on hybrid PV-wind renewable systems in the presence of electric vehicle charging stations [29]. The ANN is, in particular, a computational model composed of artificial "neurons", loosely inspired by the simplification of a biological neural network. Using machine learning, they can reproduce the behaviour of any system from the simplest to the most complex. This learning can take place either through experimental data or from numerical simulations. Experimental data are suggested to build an ANN characteristic of the physical reality of the considered system.

Literature gap and research contribution

A search in scientific databases has shown how there is still little use of this technique in the field of green roofs: only six research works have coupled the artificial intelligence model and green roof analysis. For example, Wei *et al.* predicted the roof outer surface temperature under a green roof soil layer of a building in winter in a subtropical Wuyishan city (China) using the neural network modelling method [30]. Tsang and Jim trained an ANN to predict soil moisture based on daily weather variables to determine the irrigation time and watering volume. Furthermore, to assess the

performance of artificial intelligence in green roof irrigation, two experimental plots were set up on the roof of the Main Library at the University of Hong Kong [31]. Similarly, Pandey *et al*. trained an ANN to learn to predict the reduction in heat gain from the roof buildings with the different experimental data extrapolated in the Sustainable City, Ujjain (India) [32]. Erdemir *et al.* presented an ANN model to predict temperature decrease on a green roof using training data taken from nine different cities around the world (1. London, England; 2. Montreal, Canada; 3. Moscow, Russia; 4. Athens, Greece; 5. Beijing, China; 6. Riyadh, Saudi Arabia; 7. Hong Kong, China; 8. Mumbai, India; 9 Brasilia, Brazil), characterized by different climatic conditions [33]. He *et al.* developed fifteen ANN models compared to water vapour diffusion models and data from an experimental campaign for the determination of the hourly evapotranspiration rate in Singapore [34]. Asadi *et al.* built a multilayer feed-forward neural network to find a relationship between land surface temperature and various urban characteristic parameters simultaneously in Austin, Texas [35]. Abdalla *et al.* applied four machine learning models, commonly used in runoff modelling studies, to simulate runoff from 16 green roofs located in four Norwegian cities with different climatic conditions [36].

The analysis of these few research works highlights that to date attention has been given to specific individual aspects influencing the green roof performance such as irrigation and the evapotranspiration phenomenon and to specific thermal quantities, with the surface temperature the most frequent. In addition, the cooling period is predominant as the season selected for their evaluation. However, except for the work of Erdemir *et al*. [33], no research is yet available that couples the ANN concept to the evaluation of all the main thermal parameters that intervene in the green roof performance.

To cover this research gap, this work proposes an algorithm code based on ANNs able to predict the thermal performance of a green roof on the basis of monthly values of climatic variables. Specifically, the idea behind this study is to apply ANNs to learn the thermal response of a green roof deriving from the joint action of all different thermal forcings. In detail, the tool developed trained with monthly data is able to predict the monthly external and internal green roof surface temperatures and internal air temperatures.

All these quantities are also strictly correlated to the UHI, the indoor thermal comfort, and cooling load transferred indoors. Consequently, the tool proposed here can also contribute to assessing the impact that green roofs have on these phenomena and aspects.

To achieve the purpose of the study, different green roofs were considered located in the city of Palermo, characterized by a Mediterranean climate, by varying the most important vegetation and soil parameters. The ANN was trained and validated on the basis of monthly data of external climatic conditions and other monthly green roof thermal performance indicators. The monthly data derives from dynamic hourly simulations. Training and validation data derive from an extensive parametric analysis performed by the present authors using Design Builder Software.

2. Materials and methods

The development of the green roof ANN is based on the following steps:

1) Database creation: a step consisting of gathering input and output data to create input-output pairs that will be used for the subsequent training and validation steps of the implemented ANN;

2) ANN training and optimization: a step related to the insertion of input and output data collected in the previous step to train the ANN, choose the ANN architecture and optimize the performance of the ANN chosen;
3) ANN validation: a step in which the optimized ANN is used for new predictive analyses with new data never encountered before in the training phase. To be able to use the network, it must expose the appropriate values of dome accuracy indices.

Figure 1 presents an overview of these steps implemented in the study presented here to achieve the objectives of the research.

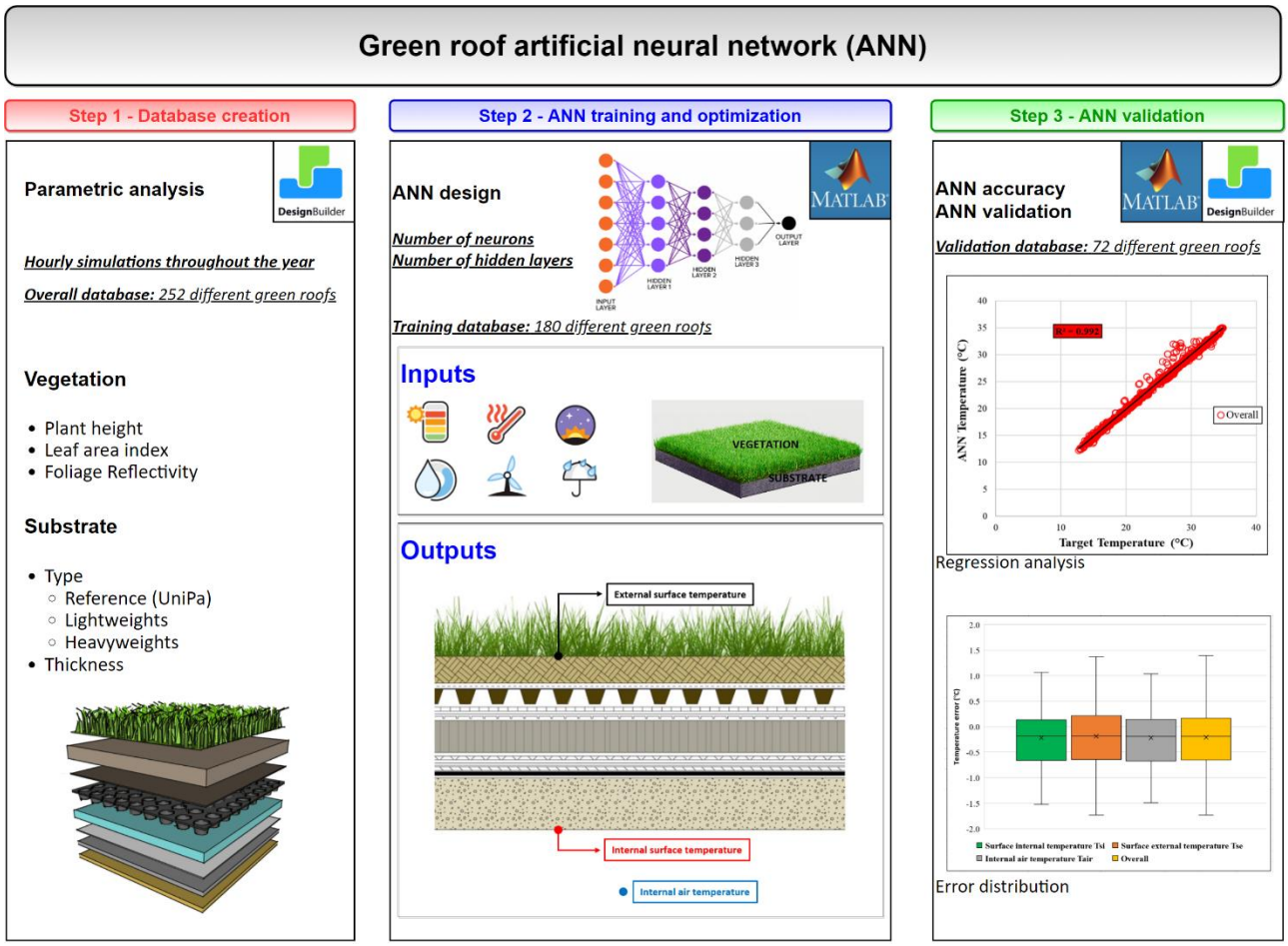

Figure 1. Overview of the different steps implemented to develop an Artificial Neural Network for the dynamic simulation of the thermal performance of a green roof in the Mediterranean climate.

2.1. Step 1 – Database creation

The first step aims to create a database that consists of all inputs affecting the green roof's thermal performance and all outputs that describes its thermal response. To generate this database, parametric simulations were carried out considering an existing green roof located in Palermo. The simulations were performed using the DesignBuilder software [37] by varying the main green roof parameters.

2.1.1. Description of the reference green roof and climatic conditions

In this research, a building located within the University of Palermo and belonging to the Department of Engineering was considered as a reference case. In particular, this building has been chosen

because on it there are three different experimental plots of green roof, which share the same stratigraphy (except for the type of vegetation planted), so it was possible to model one of them.
As for the building analysed, it has four floors and a basement (Figure 2) and is made up of laboratories and technical rooms with a ceiling height of 3.5 m. This building is characterized by a framed structure with tuff brick infill and a flat roof consisting of concrete and brick. The fixtures, which characterize the transparent elements, are made of double glazing with air with an aluminium frame and internal blinds. Hereafter, a description of the building use is described in the real building space operating. The blinds are only open on working days from April to September [38].
The building is occupied on weekdays (Monday through Friday) from 8:00 am to 6:00 pm. The lighting is provided by fluorescent lamps of varying wattage and is programmed from October to November (from 2:00 p.m. to 6:00 p.m.) and from December to March (from 8:00 a.m. to 6:00 p.m.) while for the remaining months of the year (April to September) there is natural lighting. The heating systems consist of radiators and fan coils, which are switched on from 7 a.m. to 12 p.m. and from 3 p.m. to 6 p.m. during the heating season. For cooling and heating, the setpoints were set at 25 °C and 20 °C, respectively [38].
The main thermo-physical properties of both opaque and transparent elements concern:

- external wall thickness 36 cm with transmittance 2.635 W/(m^2 K);
- double glass with air layer (4 mm - 12 mm - 4 mm) with transmittance 2.725 W/(m^2 K);
- roofing thickness 32.5 cm with transmittance 1.756 W/(m^2 K);
- green roof thickness 53 cm and transmittance 0.363 W/(m^2 K).

As for the three experimental green roofs installed on the building roof, among the different Italian patented commercial systems, PerliGarden by Perlite Italiana Srl, was used to realize the green package.

Figure 2. The front view (left) of the building of the Department of Engineering, located within the University of Palermo and the three zones (right) on the terrace selected for the installation of the green coverings, taken from [38].

Figure 3 shows the three plots on the roof of the selected building [39].

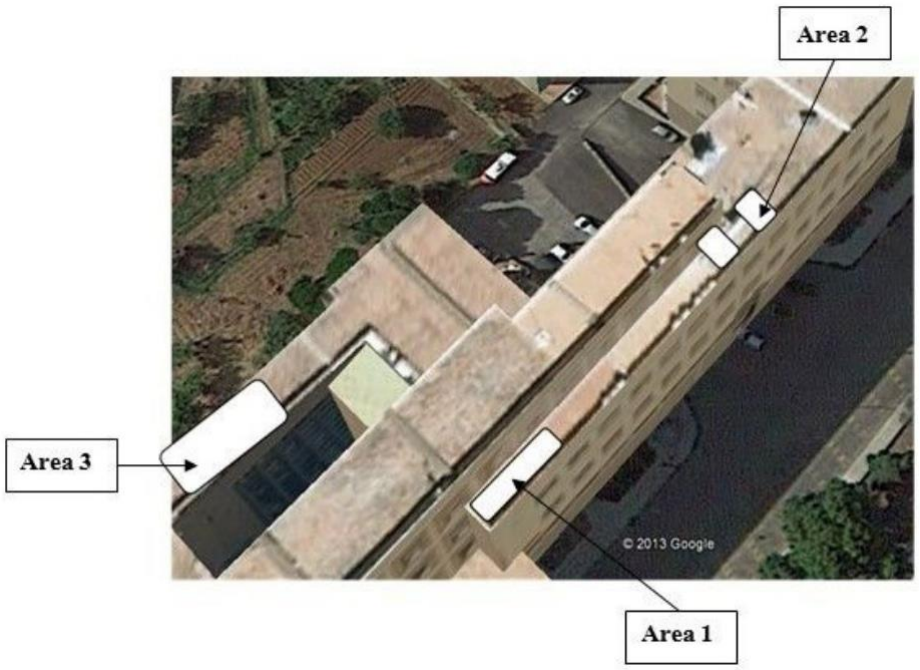

Figure 3. Positioning of plots 1, 2 and 3 on the roof of the selected building. Taken from [39].

The stratigraphy characterizing all three plots, from the outside to the inside, is the following [38-42]:

- Vegetation layer;
- Medium growing layer consisting of a mixture of lapillus, pumice, peat and slow-release fertilizers;
- Non-woven geotextile felt 100 % polypropylene calendered that constitutes the filtering element for the stratigraphy of green surfaces;
- Water storage layer composed of cushions 5 cm thick. They are made of a special calendered non-woven polyester geotextile, filled with hygroperlite or expanded perlite with a grain size of 1 ÷ 3 mm;
- Draining layer which is a composite product characterized by a polyethene geotextile hot coupled with a non-woven geotextile with filtering action;
- Waterproofing covering the role of root barrier, 5 mm thick, in a particular bituminous sheath;
- Structural support consisting of a 10 cm layer of light concrete, a 20 cm concrete slab and a 2 cm layer of plaster.

As for the vegetative layer, as shown in area 1 of Figure 4 it was decided to partition it into four sectors: the first two were planted with *Phyla nodiflora*, the third with *Gazania nivea* and the fourth was left without vegetation. In area 2, only one plant species was planted: *Gazania nivea*. Finally, area 3 was partitioned into three sectors, respectively planted with *Sedum*, *Mesembryanthemum barbatus* and *Aptenia lancifolia*. It should be noted that to decrease the growth time of the vegetation cover in the three areas, their scions were planted directly [38-40].

In addition, different thicknesses of average growing medium were taken, specifically, a 10 cm one for the vegetation cover in areas 1 and 2 and a 5 cm one for vegetation in area 3. Drip irrigation, with a rate of 3 cm/week, was chosen for these areas to achieve greater uniformity of water supply, which should help facilitate the growth of the plant species despite the limited thicknesses of the substrates [38-40].

(Area 1) (Area 2) (Area 3)

Figure 4. Planting of plots 1, 2 and 3 located on the selected building of the University of Palermo. Taken from [39].

The climatic conditions considered for the database creation are those of Palermo in Sicily, Italy, characterized by a latitude of 38° 10′ 50.14″ North, a longitude of 13°05′ 46.87″ East and an altitude of 34 meters a.s.l.
The EnergyPlus Weather File (EPW) format was used as a source of generation of climatic data of Palermo. Figure 5 illustrates the pertinent monthly average, minimum and maximum value of temperature, humidity, wind speed and global horizontal solar radiation.

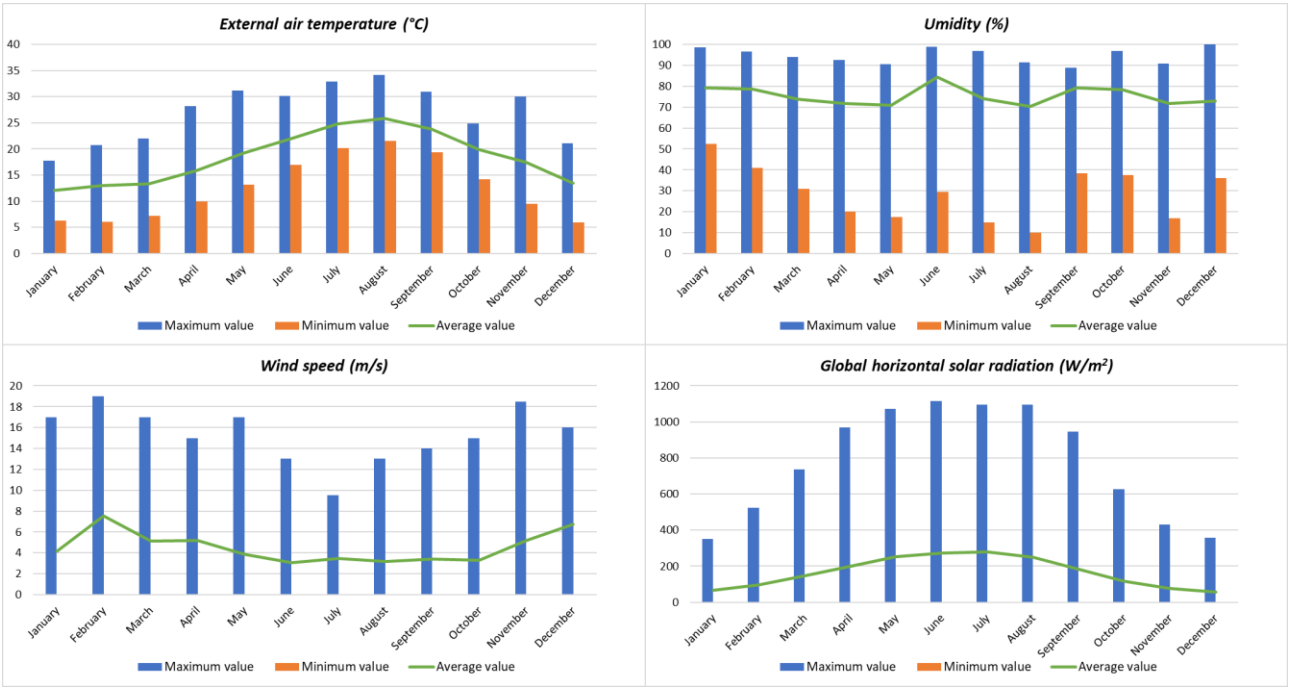

Figure 5. Monthly average, minimum and maximum value of temperature, humidity, wind speed and global horizontal solar radiation of Palermo.

As it can be seen from the figure on the top left, the months of July and August are those in which the highest temperature values are recorded; instead, the lowest ones, even negative, are recorded in the winter months (December and January). In detail, the average annual temperature is 18.41 °C, the maximum annual temperature value is 34.20 °C recorded on August 5 at 10:00 am while the minimum annual temperature value is 5.95 °C recorded on December 22 at 6:00 am.

As can be seen from the figure on the top right, the relative humidity values are mainly concentrated between 20% and 95%, but there are days when the relative humidity values go beyond this range. In detail, the average annual relative humidity is 75.42%, the maximum annual value of relative humidity is 100% recorded on December 2 at 05:00 am and the minimum annual value of relative humidity is 10% recorded on August 5 at 6:00 am.
As can be seen from the figure on the bottom left, the trend of wind speed values is extremely variable. In particular, the average annual wind speed is equal to 4.51 m/s, the maximum annual value of the wind speed is equal to 19.00 m/s recorded on February 16 at 17:00 while the minimum annual value of the wind speed is equal to 0.00 m/s which is recorded in different days during the year.
As can be seen from the figure on the bottom right, the annual mean total horizontal solar radiation is 116.96 W/m^2, while the annual maximum value is 1116.38 W/m^2 recorded on June 22 at 13:00.

2.1.2. Dynamic thermal modelling of the green roof in DesignBuilder

For the analysis of the energy performance of the green roof described and for the realization of a database to be used with neural networks was used the thermophysical model contained in the simulation program in the dynamic regime EnergyPlus-DesignBuilder [37] which is based on the model proposed by Sailor [18], previously cited. This software allows extrapolating, as an output, the heat inputs transmitted through the various building components of the envelope (walls, roof and floor), solar gains, radiant exchanges through the surfaces of the envelope, as well as the surface temperature of the individual walls, the temperature of the air inside the envelope, radiant and operating temperature.
The model under consideration is based on that of the Army Corps of Engineers' FASST [19, 43], with some modifications and assumptions made, that is:

- plants and growing medium are horizontally homogeneous;
- heat and mass transfer are analyzed according to the vertical direction only, while horizontal fluxes are negligible; this assumption implies the choice of a one-dimensional model;
- the photosynthesis phenomenon in plants is negligible in the energy balance equation;
- heat transfer by conduction in plants is negligible;
- the crop substrate is considered equivalent to a homogeneous and isotropic continuum, so its properties do not depend on direction;
- neglected thermal inertia of the substrate;
- thermal conductivity of the soil constant;
- simplified mass equation with heat flux due to vertical water transport in the soil neglected;
- crop substrate partially covered by vegetation;
- neglected precipitation flux.

The model under consideration is centred on two balance equations at the vegetation-outdoor environment interface and at the soil-outdoor environment interface, which are linearized and solved simultaneously, thus obtaining the soil (T_g) and foliage (T_f) temperature values, expressed in Kelvin. In Figure 6, a representation of the thermal exchanges between the vegetation, soil and external environment, taken into consideration by the model developed by Sailor, are shown.

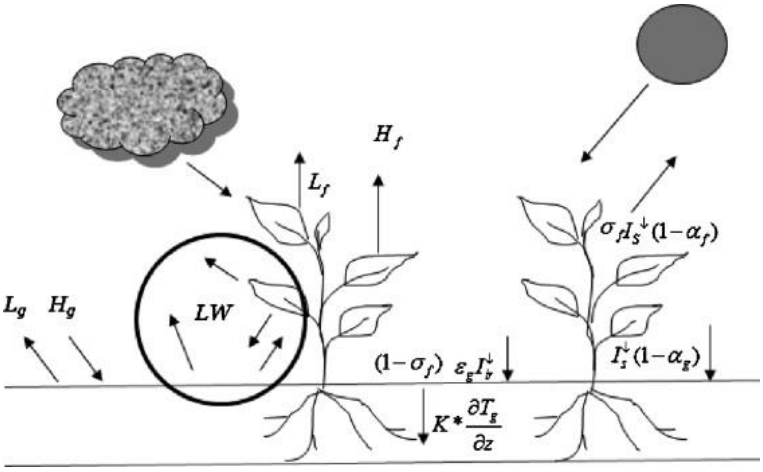

Figure 6. Representation of the thermal exchanges between vegetation - soil – external environment taken into consideration by the model developed by Sailor. Taken from [18].

In Figure 6, H_g is the soil sensible heat flux, H_f is the foliage sensible heat flux, L_g is the latent heat flux of the soil, L_f is the latent heat flux of foliage, LW is the longwave radiation and I_s is the total incoming shortwave radiative flux. The balance equation related to the foliage layer is represented by Eq. (2).

$$F_f = \sigma_f[I_s(1-\alpha_f) + \varepsilon_f I_{ir} - \varepsilon_f \sigma T_f^4] + \frac{\sigma_f\, \varepsilon_g\, \varepsilon_f\, \sigma}{\varepsilon_g + \varepsilon_f - \varepsilon_f \varepsilon_g}\left(T_g^4 - T_f^4\right) + H_f + L_f = 0 \qquad (2)$$

Where, F_f is the net foliage heat flux, I_s is the total incoming shortwave radiative flux, I_{ir} is the total incoming longwave radiative flux, α_f is the shortwave albedo of vegetation, ε_f is the long-wave emissivity of the vegetation, ε_g is the emissivity of the ground surface, σ is the Stefan-Boltzmann constant, σ_f is the fraction of vegetation cover dependent on the leaf area index (LAI) that represents, also mentioned as foliage density, the total area of leaves on only one side above a unitary ground area.
The balance equation related to the soil layer is represented by Eq. (3).

$$F_g = (1-\sigma_f)\left[I_s\left(1-\alpha_g\right) + \varepsilon_g I_{ir} - \varepsilon_g \sigma T_g^4\right] - \frac{\sigma_f\, \varepsilon_g\, \varepsilon_f\, \sigma}{\varepsilon_g + \varepsilon_f - \varepsilon_f \varepsilon_g}\left(T_g^4 - T_f^4\right) + H_g + L_g + k\frac{\partial T_g}{\partial z} = 0 \qquad (3)$$

Where, F_g is the net heat flux at the ground surface and α_g is the shortwave albedo of the ground surface, k is the soil thermal conductivity, and z is the soil depth direction.
To study the green roof thermal response, a cavity composed of adiabatic walls (see Figure 7), except the roof, was built in the DesignBuilder environment to isolate the only green roof thermal effect on the variation of the internal air temperature and internal surface temperature. In other words, to cancel the contribution of all vertical walls and floor of the cavity, the combined use of the "adiabatic" boundary condition and a reduced thickness of insulation of 0.1 cm was implemented in Design Builder. The insulation layer has the thermal and optical characteristics reported in Table 1. In this way, the incidence of the walls constituting the cavity and internal heat gains on the thermal balance of the air node is completely negligible since the energy transferred from the internal environment to the external environment and, vice versa, through the five walls is almost nil.

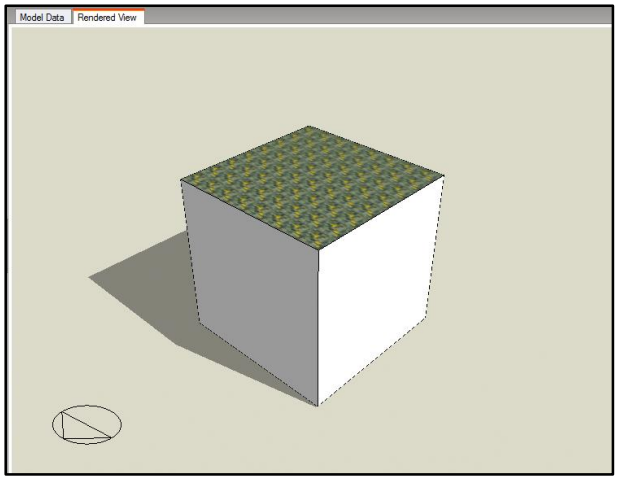

Figure 7. Rendered representation of the modelled adiabatic cavity.

Table 1. Thermophysical and optical properties of the insulation material.

Thermophysical properties of the material				**Surface optical properties**		
Insulation layer	**Thermal conductivity (W/mK)**	**Specific heat capacity (J/kgK)**	**Density (kg/m^3)**	**Emissivity (-)**	**Solar Absorbance (-)**	**Visual Absorbance (-)**
	0.001	100	20	0.99	0.01	0.01

In addition, neither internal heat gains nor window components within the cavity were considered to avoid their influence on the internal air fluctuation. In all these conditions, the cavity with the green roof installed was dynamically simulated in a free-floating regime to detect the thermal response in therms of indoor and outdoor temperature fluctuations in the absence of an air-conditioning system.
The stratigraphy of the experimental green roofs placed on the building under study, from the outside to the inside, was described in Section 2.1.1 and reproduced in DesignBuilder. In addition, DesignBuilder calculates the convective and radiative heat transfer coefficients for heat transfer of the outer and inner surfaces. The values obtained are 19.58 W/(m^2 K) and 8.77 W/(m^2 K), respectively, for the external and internal convective coefficients, and 5.41 W/(m^2 K) and 1.23 W/(m^2 K) for the external and internal radiative coefficients.
In Table 2, the thermophysical properties and the thicknesses of all green roof layers implemented in DesignBuilder are reported.

Table 2. Green roof stratigraphy description.

Stratigraphy elements	**Modelling**	**Thermophysical properties of the material**			**Thickness**
		Thermal conductivity λ (W/m K)	**Specific heat capacity c_p (J/kg K)**	**Density ρ (kg/m^3)**	**(m)**
1. Growing medium layer. It consists of a mixture of lapilli, pumice, Agrilit	Soil layer + vegetation	0.2	1100	950	-

expanded perlite, peats, bark, coconut fibres, special clays, soil conditioners, and organic fertilizers.					
2. Filter layer	100% Polypropylene	0.22	1800	910	0.05
3. Water storage layer (5-cm cushions) filled with hygroperlite or expanded perlite with a grain size of 1 to 3 mm	Bulk expanded perlite in 0.1 to 2.3 mm granules	0.05	1000	950	0.05
4. Drainage layer	Geonet in high density polyethylene coupled with a woven not woven in polypropylene	0.5	1800	980	0.045
5. Waterproofing - bituminous sheathing	Sheet/Felt Bitumen	0.23	1000	1100	0.005
6. Lightweight concrete screed	Closed structure concrete of expanded clays	0.65	1000	1600	0.10
7. Cement mortar	Cement mortar	1.400	1000	2000	0.02
8. Reinforced concrete layer	Concrete reinforced with 2% steel	2.50	1000	2400	0.20
9. Interior lime and gypsum plaster layer	Lime plaster and gypsum plaster	0.7	1000	1400	0.02

On the internal side of the roof, the emissivity was set equal to 0.9, and the solar and visible solar absorptance to 0.7. The thermophysical properties of various layers were found by referring to both the data sheets relating to the Italian patented commercial system, or PerliGarden of Perlite Italiana Srl [42], as well as some standards [44-48]. Based on these data, the overall roof steady thermal transmittance resulted to be 0.443 W/m^2 K.

2.1.3. Parametric analysis

An extensive parametric simulation was performed by changing some characteristics of the reference existing green roof stratigraphy in Palermo. In detail, starting from this stratigraphy, other green roofs were defined in DesignBuilder by varying characteristic parameters of vegetation and substrate layers in order to generate the ANN database. In particular, the typical values and the variation range of the vegetation parameters essential to performing the simulation of the building modelled in Design Builder are reported in Table 3 [49].

Table 3. Typical values and the variation range of the vegetation parameters.

Vegetation Parameter	Definition	Variation range
Plant height	Average height of plants on the green roof	0 - □ (m)

Leaf air index (LAI)	Expected leaf area per unit area of the ground surface	0.01 - 5.0 (-)
Foliage Reflectivity	Fraction of solar radiation that is incident to and then reflected from the surface of the individual leaf. Solar radiation includes the visible spectrum and infrared and ultraviolet wavelengths	0.1 - 0.4 (-)
Leaf Emissivity	Ratio of the thermal radiation emitted by the leaf surface to that emitted by an ideal black body at the same temperature. This parameter is used to calculate the radiant wavelength exchanged by the leaf surface	0.8 - 1.0 (-)
Minimum stomata resistance	Resistance of stomata to moisture transport. A cover made with plants with low stomatal resistance values will result in higher rates of plant evapotranspiration	50 - 300 (s/m)
Maximum moisture in saturation	Maximum volumetric moisture content of the soil that depends on the soil properties and, in particular, the porosity	0 – 100 (%)
Residual moisture	Minimum possible volumetric moisture content of the soil layer	0 – 100 (%)
Initial moisture	The volumetric moisture content of the soil layer at the beginning of the simulation. The moisture content is updated throughout the simulation based on surface evaporation, irrigation, and precipitation	0 – 100 (%)

Table 4 lists the parameters changed in the parametric simulation and their values considered.

Table 4. Variation range of vegetation parameters in the parametric simulation.

Parameters	Variation range	Variation step	Values considered		
Plant height (m)	0 - 0.6	0.3	0.01	0.3	0.6
Leaf air index (LAI)	0.001 - 5	2.5	0.001	2.5	5
Foliage Reflectivity	0.1 - 0.4	0.1	0.2	0.3	

Instead, the leaf emissivity and minimum stomatal resistance were considered unvaried in all simulations and equal to 0.95 and 180 s/m, respectively.

In addition, substrates different to the one implemented in the reference green roof were considered to study the effect produced by the thermophysical properties and thickness of the substrate layer on the green roof thermal response.

Besides the growing substrate of the experimental green cover placed on the building of the University of Palermo consists of a mixture of lapillus, pumice, Agrilit expanded perlite, peats, barks, coconut fibres, special clays, soil conditioners, organic fertilizers, other types of soil substrates were considered [50, 51]. Specifically, to study how the thermal properties of the growing medium and moisture content affect the energy performance of the green cover, lightweight and heavyweight substrates were analyzed [50, 51].

The constituent materials of the lightweight substrate are pumice (75 %), compost (10 %) and sand (15 %), while those of the heavyweight substrate are expanded shale (50 %) and sand (50 %).

The lightweight substrate is characterized by the highest moisture capacity, lowest thermal conductivity, and lowest density among all substrates, while the heavyweight one has the highest density and thermal conductivity among substrates.
To determine the influence of substrate moisture content on the energy performance of vegetated covers, the thermal properties of each growing medium were considered for three different percentage moisture content levels: 20%, 60% and 100% taken from the literature [50, 51].
Table 5 reports all thermophysical data of the different additional substrates considered for different values of the moisture content.

Table 5. Thermal properties of lightweight and heavyweight substrates for three different moisture contents.

Substrate number	**Moisture contents (%)**	**Density ρ (kg/m^3)**	**Thermal conductivity λ (W/mK)**	**Specific heat capacity c_p (J/kgK)**
		Lightweight substrate		
1	20	765	0.21	1284
2	*60*	*870*	*0.31*	*1602*
3	100	934	0.41	1853
		Heavyweight substrate		
4	20	1385	0.37	936
5	*60*	*1450*	*0.6*	*1035*
6	100	1500	0.84	1095

As it can be seen, the thermal conductivity λ and density ρ increase as substrate moisture content. In addition, the specific heat c_p increases as moisture content increases since water has a greater thermal storage capacity than air. Finally, two different substrate thicknesses of 0.1 and 0.3 m were considered.
For the reference soil, also the maximum volumetric moisture content at saturation, minimum residual volumetric moisture content and initial volumetric moisture content, in all simulations, were set the same and equal to 0.42 m^3/m^3, 0.05 m^3/m^3 and 0.21 m^3/m^3, respectively. Instead, for the lightweight and heavyweight soils, the previous three parameters were set equal to 0.5 m^3/m^3, 0.01 m^3/m^3 and 0.2 m^3/m^3, respectively.
Overall, 18 different vegetation layers, 7 different substrate layers and two substrate thicknesses were considered. The parametrical analysis consists of hourly simulations throughout the year of 252 different green roofs. For each hourly simulation, the hourly inputs are represented by the climatic conditions, while the hourly outputs are represented by the internal air temperature, internal and external surface temperature and internal and external surface heat flux.
To extract from this database data for the training and validation phases, the reference soil resting on top of the building of the University of Palermo and, among the six additional cultivation soils, those with the most extreme thermal properties, *i.e.* characterized by the highest and lowest values of thermal conductivity (W/(m K)), specific heat (J/(kg K)) and density (kg/m^3) were selected for the training phase. The remaining two substrates were used for the ANN validation phase. Table 5 highlights the substrates selected for the validation phase in underlined italics.

2.2. Step 2 - Artificial neural network (ANN) training and optimization

2.2.1. What is an ANN?

The biological neural system consists of neurons, which in turn consists of the soma, from which a series of ramifications, called dendrites and a central body called axon from which other ramifications, called axon terminals, start, which have a swelling, the so-called synaptic button. The neuron has the function of receiving, integrating and transmitting nerve impulses; it receives information from the external environment in the form of an electrical signal. This signal reaches the neuron through dendrites, which transmit the information to the pack. In the soma, an integration process takes place, *i.e.* all the information coming from the various dendrites are added together and if a certain threshold value, called the potential threshold, is exceeded, the new signal is transmitted to the other neurons. The synaptic buttons of an axon are in contact with the dendrites of other neurons in such a way that the nerve impulse propagates along the neuronal circuit. The connection between neurons is called the synapse, which can be either excitatory or inhibitory depending on whether it favours or inhibits the transmission of the electrical signal between the neurons.

The functioning of ANNs simplifies what happens within the biological neural system. Specifically, an ANN is made up of elementary units, the artificial neurons, between which some connections simulate synapses between biological neurons. Each neuron processes the received signals and transmits the result to other neurons through the connections. The importance is not the same for all connections but is determined through a connection weight, attributed to each connection between neurons. The ANN framework shown in Figure 8 simulates the behaviour of the biological neuron.

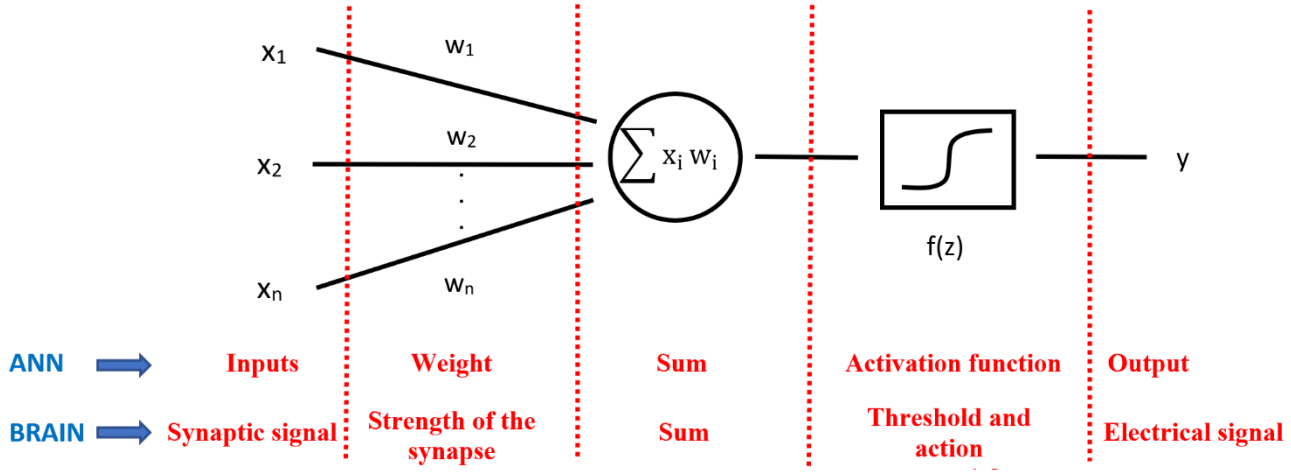

Figure 8. Framework of ANN reproducing brain neuron behaviour

On the left, the inputs correspond to the synaptic signal coming from the dendrites to the biological neuron. Each signal has a weight (w) which represents the force of the synapse. In the central part, a weighted sum of the various inputs with their respective weights is performed, as it happens in the biological neuron soma. This sum must exceed a certain threshold, which takes the name of the activation function, which corresponds to the potential threshold of the biological neuron.

Different ANN architecture types are available based on the number of input and output neurons and based on their connection. The neurons are organized in layers. In particular, neurons belonging to the same layer present similar behaviour. It is necessary to mention that the input nodes are not considered layers since they are not involved in processing. According to [52], the ANN can be classified according to its architecture in (i) single-layer feedforward ANNs, composed of a layer of

input neurons and a layer of output neurons, in which the propagation of the signal occurs only in one direction, from the input layer to the output layer and, therefore, it is strongly acyclic or feedforward; (ii) multilayer feedforward ANNs, characterized by the presence of one or more layers of hidden nodes (hidden layers) placed between input nodes and output nodes, in which the operation takes place only in one direction from input to output and the final efficiency of the model is greater than the single-layer ANN; and (iii) recurrent ANNs, characterized by at least one feedback or a counter-reaction cycle, in which there is a level of neurons that sends the output signals back to the input and the learning capacity is enhanced.

2.2.2. ANN elements and equations

Generally, an ANN consists of three basic elements:

- a set of synapses or connections each of which is characterized by a weight (synaptic efficacy); unlike the human model, the artificial model can have both negative and positive weights;
- a summation that sums the signals in input weighed by the respective synapses, producing in output a linear combination of the inputs;
- an activation function to limit the amplitude of the output of a neuron. Typically the amplitude of the outputs belongs to the range [0,1] or [-1,1].

The neuronal model also consists of a threshold value that has the effect, depending on its positivity or negativity, of increasing or decreasing the net input to the activation function.
This model undergoes a learning process in which the weights are gradually updated until the mean square error between the output of the ANN (Output) and the desired output (Target) is minimized.
In mathematical terms, a neuron k is described with Eqs. (4) and (5).

$$u_k = \sum_{j=0}^{m} w_{kj} \, . \, x_j \tag{4}$$

$$y_k = \varphi(u_k + b_k) \tag{5}$$

Where, x_j are the inputs relative to neuron k, w_{kj} is the j-th synaptic weights of neuron k, u_k is the linear combination of the inputs in neuron k, b_k is the threshold value of neuron k, $\varphi(x)$ is the activation function and y_k is the output generated by neuron k.
The elements that characterize an ANN result are: input level; hidden level/s; output level; weights and distortions between levels; function of activation.
The type of activation function used determines the neuron's response. In the literature, different types of activation functions are employed. The most used are:

1. *Step activation function (Heaviside function)*

   The step activation function f(A) of Eq. (6) assumes value 1 if the weighted sum is greater than the threshold value s; otherwise, it assumes value 0.

$$f(A) = \begin{cases} 1 & \text{if } A \geq s \\ 0 & \text{else} \end{cases} \tag{6}$$

2. *Sign step activation function*

The sign activation function of Eq. (7) assumes value 1 if it is greater than the threshold value, otherwise, it assumes value -1.

$$f(A) = \begin{cases} 1 & \text{if } A \geq s \\ -1 & \text{else} \end{cases} \quad (7)$$

3. Continuous linear activation function

The continuous linear activation function of Eq. (8) is directly proportional to the weighted sum of the input signals and when ε=1 is equal to this weighted sum.

$$f(A) = \varepsilon A \quad (8)$$

The previous activation functions are all continuous functions. This allows the transmission of signals of gradual intensity and makes them similar to biological neurons. In addition, there are also widely used non-linear continuous activation functions.

4. Binary sigmoidal activation function

The binary sigmoidal activation function of Eq. (9) is an increasing function and varies in the interval [0, 1].

$$f(A) = \frac{1}{1 + e^{-\varepsilon A}} \quad (9)$$

where ε indicates the slope of the function. When ε = 1 the Log-sigmoid activation function is obtained.

5. Bipolar sigmoidal activation function

The bipolar sigmoidal activation function of Eq. (10) varies in the interval [1, -1] and uses the hyperbolic tangent:

$$f(A) = \tanh(\varepsilon A) \quad (10)$$

where ε represents the slope of the function. When ε=1, the hyperbolic tangent sigmoid activation function of Eq. (11) is obtained.

$$f(A) = \frac{2}{1 + e^{-2A}} - 1 \quad (11)$$

Figure 9 shows all the activation functions described.

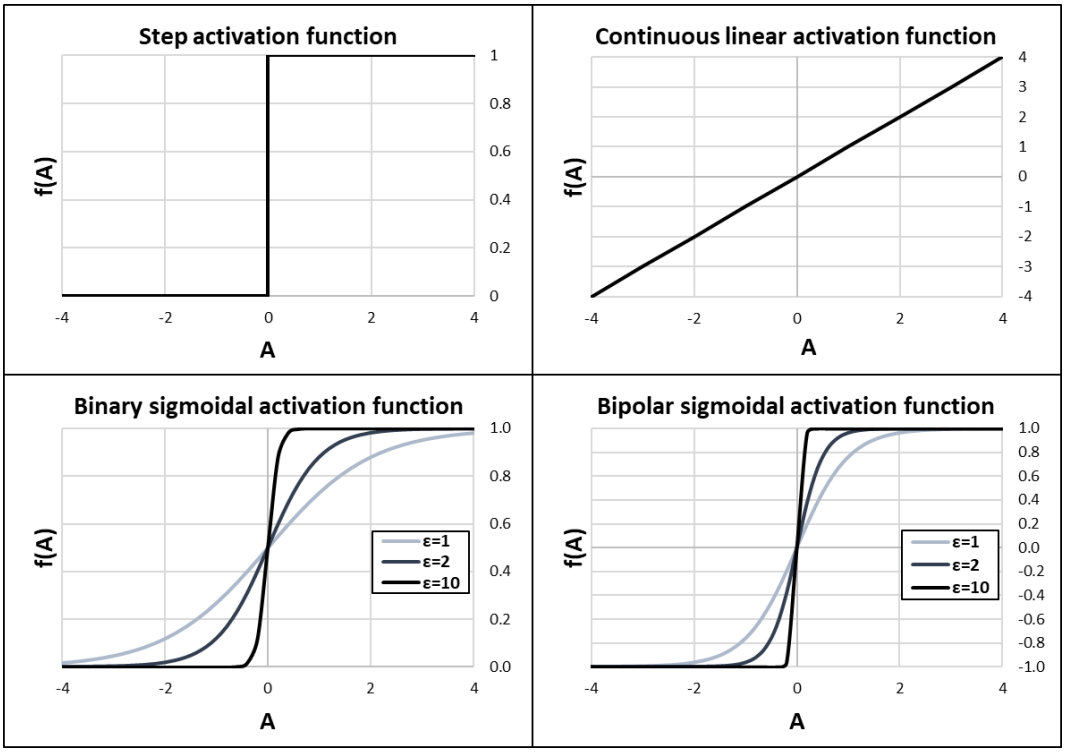

Figure 9. Most employed activation functions.

In this research work, hyperbolic tangent sigmoid activation functions were used in the hidden layers, while a continuous linear activation function was associated with the output layer. The advantage of using hyperbolic tangent sigmoid activation functions in the hidden layers is that the negative inputs will be mapped strongly negative and the zero inputs will be mapped near zero. In addition, the function is differentiable and monotonic while its derivative is not monotonic. All these characteristics are very useful for the training algorithm, explained in the successive section, to know in which direction and how much to change or update the ANN weights. Instead, the continuous linear activation function does not alter the output from the ANN.

2.2.3. ANN training algorithm

To build an effective ANN model, it is necessary to carry out an ANN training phase in which the model receives a series of input data, apparently unrelated to each other, and a series of outputs, to learn the relationship between input and output. These data are numerically or experimentally analyzed and elaborated by experts and the data produced constitute the model outputs.

In the training phase, the ANN learns the relationships existing between the inputs, which are the data collected, and the outputs, which are the evaluations made by the experts. The training phase aims to provide an output solution even when different input data are provided. In particular, the ANN training phase can be based on three different algorithms: supervised, unsupervised, and reinforcement. Supervised learning is used to solve classification and regression problems, and the objective is to learn the relationship between inputs and outputs given as training data. Then the ANN generalizes this relationship by processing correct outputs even when it receives different data inputs. In particular, the ANN increases the weights that provide a correct solution and decreases those that provide an incorrect solution.

Several ANN learning methods were developed to speed up the learning process. The four following training algorithms are the most commonly used:

- Error back-propagation algorithm: is a decreasing gradient method that optimizes the value of the weights minimizing the total square error between the ANN output (output) and the desired output (target) [52].
- Levenberg-Marquardt algorithm: requires more memory but less time. The training phase stops automatically when the generalization stops improving, i.e. when there is an increase in the mean square error (MSE) of the validation samples.
- Bayesian Regularization: allows for achieving a good generalization in the case of difficult, small or noisy datasets, at the expense of a longer training time.
- Scaled Conjugate Gradient: the training phase stops automatically when the generalization stops improving, as in the Levenberg-Marquardt algorithm but requires less memory.

In this research work, the Levenberg-Marquardt algorithm was used, which is widely used in ANNs because it is the most stable and fastest method in finding the solution, while the method of back-propagation of the error is valid in the case of ANNs composed of a large number of hidden layers and neurons. The Levenberg-Marquardt algorithm refers to the Newton approximation method and the Hessian matrix to assign values to weights [53-55]. It is based on both the Newton method and the gradient descent method and is an iterative regression technique used to solve multi-variable nonlinear problems. To better understand the Levenberg-Marquardt algorithm, the Descending gradient and Newton methods underlying this algorithm are summarily described.

- In the descending gradient method, the weights w are changed at step k+1 using Eq. (12).

$$w_{k+1} = w_k - \alpha g_k \tag{12}$$

  in which the constant α is called learning rate and g is the gradient with a negative sign, which is the first derivative of the function sum of the square of the errors. The problem with this method is the difficulty of choosing the learning rate α, which depends strongly on the speed with which the function converges to the minimum.
- In the Newton method, the weights w are updated at step k+1 with Eq. (13):

$$w_{k+1} = w_k - H_k^{-1} g_k \tag{13}$$

  in which H is the Hessian matrix of the second derivatives of the sum function of the quadratic error with respect to the weights. The introduction of the Hessian matrix allows the learning rate α to be adjusted at each step k, while in the previous method α is fixed. To calculate the Hessian matrix, the Gauss-Newton method is used, which modifies the weights w at step k+1 with Eq. (14).

$$w_{k+1} = w_k - \left(J_k^T J_k\right)^{-1} J_k e_k \tag{14}$$

  where J^T is the transposed Jacobian matrix which approximates the Hessian matrix using the prime derivatives and not the secondary derivatives, so the Hessian matrix is written via the Jacobian matrix as:

$$H_k = J_k^T J_k \tag{15}$$

while the gradient g is:

$$g = J^T e \tag{16}$$

where e is the ANN error vector.

In this way, the Gauss-Newton method solves the problem of slowness in finding the minimum of the sum function of the square of the errors. However, it may diverge from the solution in the case of complex problems. Instead, the Levenberg-Marquardt method modifies the weights w at step k+1 with the equation:

$$w_{k+1} = w_k - \left(J_k^T J_k + \mu I\right)^{-1} J_k e_k \tag{17}$$

Compared to the Gauss-Newton method, this method introduces the parameter μ, called the damping coefficient, and the identity matrix I. The damping coefficient is introduced to prevent the algorithm from diverging from the minimum error function. Parameter μ varies according to the following criteria: is reduced when a step in the algorithm leads to a better value of the error function, such that convergence to the minimum value is accelerated; is increased when the value of the error function moves away from the minimum so that the variation of the weights is reduced to find a better value of the error function. The iterative Levenberg-Marquardt algorithm steps used during the ANN training are: (i) starting the ANN training with random values of the weights w_k; (ii) calculation of the errors, namely a sum function of the square of the errors and Jacobian matrix; (iii) modification of the values of the weights w_k using a random value of the damping parameter μ; (iv) recalculation of the errors E and sum function of the square of the errors with the new values of the weights; (v) if the error is decreased ($E_{k-1} < E_k$), then the damping parameter μ is divided by 10 such that the speed of convergence is increased, while if the error has increased ($E_{k-1} > E_k$), then the damping parameter μ is multiplied by 10 to decrease the speed of convergence; (vi) return to step (ii). The epochs indicate the number of times the ANN is trained with the training set. The training algorithm is interrupted when the sum function of the square of the errors reaches a minimum value set as a threshold or when this function starts to increase on the percentage of data of the "validation test".

In this work, the ANN was implemented using MATLAB software, MATrix LABoratory, by means of the Neural Net Fitting tool [56]. ANN database was divided into three groups of the input data: a group, 70% of the data, was used for the ANN training of the network; the second group, 15% of the data, was used for the ANN testing, and the remaining 15% was used for the validation of the model. Once the training phase is completed, the interface returns the values of the regression coefficient R2 and the value of the mean square error MSE to evaluate the performance of the network. In case the values of the latter are not completely satisfactory, the number of neurons in the hidden layer is changed and the ANN is trained again.

2.2.4. ANN inputs and outputs

Hourly results obtained with Design Builder were synthesized at a monthly average daily level for all five soil substrates selected in the training phase.

Therefore, a "training parametric table" was created for the training phase, that is a table characterized by input-output pairs for each simulation and each month. It, in particular, is constituted by a number of columns equal to the number of the inputs and outputs considered and by a number of rows equal

to the product between the number of simulations realized for the specific substrate, that is 36, and the number of months of the year.
Table 6 lists all inputs and outputs considered for the ANN creation.

Table 6. Inputs and outputs considered for the ANN creation

Inputs	**Characteristic parameters of the soil substrate:** Density (kg/m^3) Thermal conductivity (W/(m K)) Specific heat capacity (J/(kg K)) Maximum volumetric moisture content at saturation (m^3/m^3) Thickness (m) **Vegetation characteristic parameters** Plant height (m) LAI (-) Leaf reflectivity (-) **Climatic data of Palermo** Monthly average daily dry bulb temperature (°C) Monthly average daily percentage relative humidity (%) Monthly average daily wind speed (m/s) Monthly average daily total horizontal radiation (W/m^2) Monthly average daily diffuse radiation from the sky on the horizontal (W/m^2) Monthly average daily sky temperature (°C)
Outputs	Monthly average daily internal surface temperature (°C) Monthly average daily external surface temperature (°C) Monthly average daily internal air temperature (°C)

The 14 inputs considered are related to the parameters of the vegetation, the thickness and the thermal properties of the soil substrate, as well as the climatic data of the reference city of Palermo, while the 3 outputs considered are related to the green roof surface temperatures and internal air temperature, according to Figure 10.

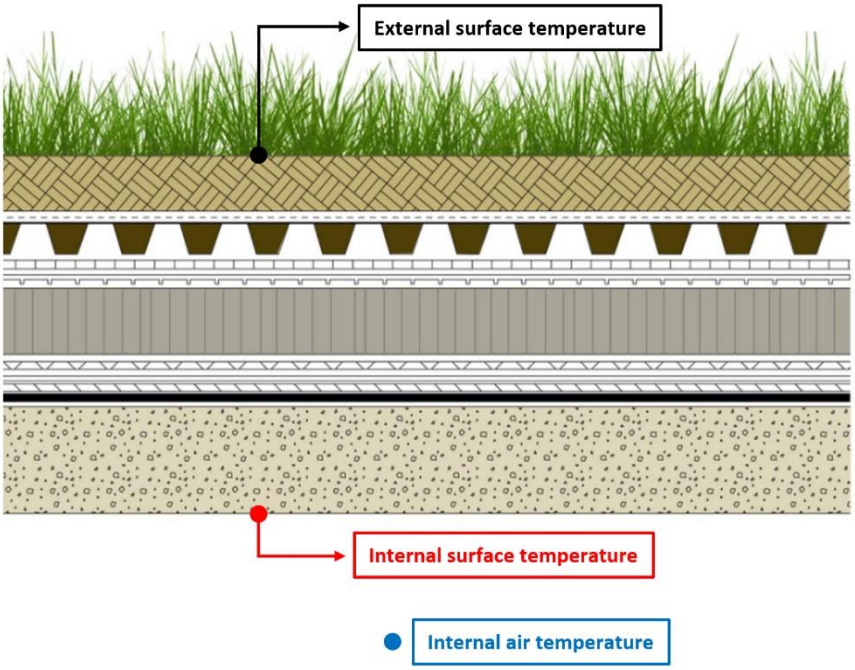

Figure 10. ANN outputs: internal and external surface temperatures of the green roof and internal air temperature.

The chosen outputs are useful to calculate the monthly average daily power entering or exiting from the external and internal surface of the green roof. At this point, it is worth noting that the external surface temperature is also directly connected to the UHI mitigation reached by implementing a green roof, while the internal temperatures are also directly connected to indoor thermal comfort.
The "training parametric table" implemented for the training phase, for a specific substrate, consists of 17 columns (14 input and 3 outputs) and 432 rows (36 simulations related to each month).
Subsequently, five "training parametric tables" were created and queued for each substrate chosen for the training phase. This allowed obtaining a "training parametric table overall" consisting of the same number of columns and 2160 rows (432 rows for five terrain substrates), that was imported into MATLAB in matrix format. Once the input data and the target data have been inserted, the tool allows selecting the percentages according to which the data are divided for the training, validation and testing phase. In particular, the percentages are: 70% of the data for training; 15% of the data for the validation in such a way that the training is interrupted when the generalization stops improving; 15% of the data for the testing phase, which does not affect training. Consequently, 1512 data were used for training, and 324 data were used for both validation and testing.
Overall, this research aims to create a monthly ANN, calculated on the basis of hourly values previously simulated with Design Builder, to predict the three temperatures mentioned in Table 6.

2.2.5. ANN optimization

The accuracy of the ANN prediction is evaluated by comparing the output values obtained using the implemented ANN with those obtained using the DesignBuilder software, which are considered as desired or target values.
Table 7 lists the statistical indices used to estimate the accuracy and precision of results provided by the monthly ANN based on hourly data [57]. Specifically, the table shows for each statistical index the calculation formula, range of variation, and optimal value.

Table 7. Accuracy metric name, equation, variation range and optimal value [57].

Accuracy metric	Equation	Range and optimal value
Mean square error (MSE)	$\mathrm{MSE} = \frac{\sum_{i=1}^{N}(t_i - y_i)^2}{N}$	$(\mathbf{0}, +\infty)$
Mean absolute error (MAE)	$\mathrm{MAE} = \frac{\sum_{i=1}^{N}\lvert t_i - y_i\rvert}{N}$	$(\mathbf{0}, +\infty)$
Root mean square error (RMSE)	$\mathrm{RMSE} = \sqrt{\mathrm{MSE}}$	$(\mathbf{0}, +\infty)$
Coefficient of variance (COV)	$\mathrm{COV} = \frac{\mathrm{RMSE}}{\frac{\sum_{i=1}^{N} {y_i}^2}{N}} \cdot 100$	$(\mathbf{0}, +\infty)$
Correlation coefficient (CC)	$\mathrm{CC} = \mathrm{R} = \frac{N\sum_{i=1}^{N} t_i\, y_i - \left(\sum_{i=1}^{N} t_i\right)\left(\sum_{i=1}^{N} y_i\right)}{\left[N\left(\sum_{i=1}^{N} {t_i}^2\right) - \left(\sum_{i=1}^{N} t_i\right)^2\right]\left[N\left(\sum_{i=1}^{N} {y_i}^2\right) - \left(\sum_{i=1}^{N} y_i\right)^2\right]}$	$(-\infty, \mathbf{1})$
R-square (R^2)	$R^2 = \frac{N\sum_{i=1}^{N} t_i\, y_i - \left(\sum_{i=1}^{N} t_i\right)\left(\sum_{i=1}^{N} y_i\right)}{\left[N\left(\sum_{i=1}^{N} {t_i}^2\right) - \left(\sum_{i=1}^{N} t_i\right)^2\right]\left[N\left(\sum_{i=1}^{N} {y_i}^2\right) - \left(\sum_{i=1}^{N} y_i\right)^2\right]}$	$(0, \mathbf{1})$
Coefficient of determination (COD)	$\mathrm{COD} = \frac{\left[\sum_{i=1}^{N}(t_i - t_m)\,(y_i - y_m)\right]^2}{\sum_{i=1}^{N}(t_i - t_m)^2 \sum_{i=1}^{N}(y_i - y_m)^2}$	$(0, +\infty)$
Efficiency coefficient (EC)	$\mathrm{EC} = 1 - \frac{\sum_{i=1}^{N}(t_i - y_i)^2}{\sum_{i=1}^{N}(t_i - t_m)^2}$	$(-\infty, \mathbf{1})$
Overall index of model performance (OIMP)	$\mathrm{OIMP} = \frac{1}{2}\left[1 - \left(\frac{\mathrm{RMSE}}{t_{max} - t_{min}}\right) + \mathrm{EC}\right]$	$(-\infty, \mathbf{1})$
Coefficient of residual mass (CRM)	$\mathrm{CRM} = \frac{\sum_{i=1}^{N} y_i - \sum_{i=1}^{N} t_i}{\sum_{i=1}^{N} t_i}$	$(-\square, +\square)$ **0**

The optimal value of the different metrics is highlighted in bold.

Where:

- t_i, t_m, t_{max} e t_{min} represent the values i-th, average, maximum and minimum of the output target obtained from the simulations carried out with the software Design Builder;
- y_i e y_m represent the values i-th and average of the output in output from the ANN;
- N represents the total number of data.

Furthermore, additional metrics (minimum, maximum, mean and standard deviation values of the error) for the accuracy of the ANN are reported below. They are related to the errors between the values of the i-th output target (t_i), obtained from the simulations carried out with the software Design Builder, and the values of the i-th output obtained with the ANN (y_i):

$$E_{min} = \min(t_i - y_i) \tag{18}$$

$$E_{max} = \max(t_i - y_i) \tag{19}$$

$$E_m = \frac{\sum(t_i - y_i)}{N} \tag{20}$$

$$E_{sd} = \sqrt{\frac{\sum(E_i - E_m)^2}{N}} \quad (21)$$

Table 7 highlights the interval of variation of these statistical indices in the third column and, in particular in bold, the optimal value. Therefore, it is easy to notice as the model that exhibits values of E_{max}, E_{min}, E_m, E_{sd}, MSE, MAE, RMSE, COV and CRM close or even equal to zero is the best from the point of view of precision and accuracy of the results predicted by the ANN with respect to the target results simulated with Design Builder; while the model characterized by values for R, R2, EC, COD and OIMP close or even equal to unity is the most accurate and precise in predicting the simulated target results [57].

These indices were used in the present research work to identify the optimal number of neurons in the hidden layer and the optimal number of hidden layers. In general, it is recommended not to set too high a number of neurons in the hidden layer because as the number of neurons in the hidden layer increases, the complexity of the network increases and therefore the computational burden. Usually, a high number of neurons in the hidden layer is set when very complex problems that have many inputs and outputs are faced. In this manner, a more effective resolution is reached. On the other hand, a high number of neurons in the hidden layer implies the risk of adapting the network in a perfect way to the data used in the training phase (overfitting), thus losing the capacity for generalization of the network.

The ANN training was developed iteratively by increasing the number of neurons evaluating each time the statistical indices of the network (in general, coefficient of determination R2 and the root mean square error RMSE) that represent the performance parameters.

In this research work, a progressively increasing number of neurons in the hidden layer was set due to the high complexity of the network under study. In particular, a study was carried out varying the number of neurons in the hidden layer from 1 to 100 in steps of 5 and from 100 to 200 in steps of 10. The final objective is to identify the optimal number of neurons in the hidden layer. Once the optimal number of neurons was identified, the ANN with a single hidden layer was compared with another ANN characterized by the same overall number of neurons divided into two hidden layers.

2.3. Step 3 – ANN validation

The validation step of an ANN represents the last step and aims to validate the final model using input data different from those used in the training phase to verify that the ANN has learned to generalize the model. If the verification is not satisfied, it is necessary to return to the training phase, while if the solution provided by the ANN is compatible with that provided by experts, the model is used with the various hardware and software. The ANN validation phase quickly provides the results obtained with the new data, even if the ANN training phase was slow. In the validation step, the ANN was used to predict the thermal performance of the other 72 green roof configurations, described in Section 2.1 and not used in the training step. The results obtained from the optimal ANN were compared with the results obtained by means of dynamic simulations performed of the same 72 green roofs in Design Builder. For this purpose, the same accuracy metrics employed in the training and optimization step and described in Section 2.2.5, were also applied in the validation step.

3. Results

In Sections 3.1 and 3.2, results obtained in the green roof ANN training and optimization phase are illustrated and results related to the green roof ANN validation phase are described.

3.1. ANN training and optimization

3.1.1. Impact of the number of neurons

Tables 8-11 show the metrics obtained in the ANN training phase for the internal surface temperature, external surface temperature and internal air temperature at the monthly average daily level, as well as for all outputs simultaneosly.

Table 8. Accuracy metrics obtained for monthly average daily internal surface temperature.

# Neurons	MAE	R^2	MSE	RMSE	EC	CRM	COV	Corr - R	COD	OIMP	E_{max}	E_{min}	E_{avg}	E_{sd}
1	1.1434	0.9426	2.0908	1.4460	0.9426	0.0007	6.4839	0.9709	0.9480	0.9392	4.2852	-6.9196	0.0165	1.4462
5	0.4691	0.9853	0.5373	0.7330	0.9853	-0.0006	3.2824	0.9926	0.9862	0.9764	2.7010	-7.6856	-0.0144	0.7330
10	0.3284	0.9940	0.2192	0.4681	0.9940	-0.0009	2.0959	0.9970	0.9941	0.9866	2.6133	-4.5244	-0.0190	0.4679
15	0.2546	0.9965	0.1270	0.3564	0.9965	0.0000	1.5969	0.9983	0.9966	0.9903	2.2744	-2.0592	-0.0009	0.3565
20	0.2097	0.9977	0.0845	0.2906	0.9977	0.0002	1.3025	0.9988	0.9977	0.9924	1.7372	-1.6458	0.0034	0.2907
25	0.1548	0.9986	0.0514	0.2268	0.9986	0.0001	1.0161	0.9993	0.9986	0.9943	2.2679	-1.4178	0.0012	0.2268
30	0.1588	0.9986	0.0528	0.2297	0.9986	-0.0002	1.0290	0.9993	0.9986	0.9942	1.5184	-2.1512	-0.0041	0.2297
35	0.1380	0.9990	0.0351	0.1873	0.9990	-0.0002	0.8390	0.9995	0.9990	0.9954	1.3513	-1.0194	-0.0034	0.1873
40	0.1354	0.9989	0.0392	0.1979	0.9989	0.0000	0.8869	0.9995	0.9989	0.9951	2.1853	-0.9478	0.0007	0.1980
45	0.1265	0.9991	0.0316	0.1778	0.9991	0.0003	0.7969	0.9996	0.9991	0.9956	1.0852	-0.8525	0.0067	0.1777
50	0.1203	0.9992	0.0291	0.1706	0.9992	-0.0004	0.7643	0.9996	0.9992	0.9958	0.7030	-1.4555	-0.0078	0.1705
55	0.1580	0.9983	0.0607	0.2464	0.9983	-0.0002	1.1036	0.9992	0.9984	0.9937	1.2458	-3.3986	-0.0050	0.2464
60	0.1084	0.9993	0.0242	0.1557	0.9993	0.0005	0.6980	0.9997	0.9994	0.9962	1.0060	-0.6942	0.0111	0.1553
65	0.1033	0.9994	0.0223	0.1492	0.9994	0.0002	0.6687	0.9997	0.9994	0.9964	0.8831	-0.7314	0.0051	0.1491
70	0.1171	0.9992	0.0281	0.1675	0.9992	0.0001	0.7505	0.9996	0.9992	0.9959	0.8131	-0.9138	0.0023	0.1675
75	0.1056	0.9993	0.0266	0.1630	0.9993	0.0001	0.7302	0.9996	0.9993	0.9960	1.4195	-1.1077	0.0020	0.1630
80	0.1277	0.9990	0.0363	0.1906	0.9990	0.0000	0.8541	0.9995	0.9990	0.9953	1.0303	-1.7636	-0.0007	0.1907
85	0.1270	0.9989	0.0386	0.1965	0.9989	0.0006	0.8808	0.9995	0.9990	0.9951	1.2756	-1.2698	0.0132	0.1961
90	0.0927	0.9994	0.0218	0.1475	0.9994	-0.0002	0.6607	0.9997	0.9994	0.9964	0.8173	-1.2033	-0.0041	0.1475
95	0.1064	0.9991	0.0341	0.1846	0.9991	0.0001	0.8273	0.9995	0.9991	0.9954	2.5874	-0.7867	0.0015	0.1847
100	0.1246	0.9990	0.0369	0.1922	0.9990	0.0005	0.8614	0.9995	0.9990	0.9952	1.5628	-1.3216	0.0108	0.1919
110	0.1302	0.9985	0.0543	0.2330	0.9985	0.0005	1.0445	0.9993	0.9985	0.9941	3.7251	-0.9689	0.0114	0.2328
120	0.1169	0.9990	0.0374	0.1934	0.9990	0.0001	0.8669	0.9995	0.9990	0.9952	2.0648	-1.9354	0.0030	0.1935
130	0.1261	0.9989	0.0394	0.1984	0.9989	0.0001	0.8890	0.9995	0.9989	0.9951	1.1668	-2.5817	0.0026	0.1984
140	0.1240	0.9989	0.0418	0.2045	0.9989	0.0004	0.9167	0.9994	0.9989	0.9949	1.8538	-0.9136	0.0096	0.2043
150	0.1179	0.9988	0.0456	0.2134	0.9987	0.0006	0.9569	0.9994	0.9988	0.9946	2.9497	-1.2934	0.0123	0.2131
160	0.1496	0.9984	0.0570	0.2387	0.9984	0.0002	1.0696	0.9992	0.9985	0.9939	2.3297	-1.4390	0.0044	0.2387
170	0.1214	0.9990	0.0362	0.1904	0.9990	0.0002	0.8532	0.9995	0.9990	0.9953	1.2806	-0.9798	0.0053	0.1903
180	0.1541	0.9982	0.0660	0.2568	0.9982	0.0005	1.1514	0.9991	0.9982	0.9934	1.4807	-1.3016	0.0115	0.2566
190	0.1647	0.9979	0.0765	0.2765	0.9979	0.0003	1.2395	0.9990	0.9980	0.9928	2.3546	-2.2985	0.0072	0.2765
200	0.1499	0.9981	0.0701	0.2648	0.9981	-0.0004	1.1860	0.9990	0.9981	0.9932	1.9779	-1.9269	-0.0094	0.2647

Table 9. Accuracy metrics obtained for monthly average daily external surface temperature.

# Neurons	MAE	R^2	MSE	RMSE	EC	CRM	COV	Corr - R	COD	OIMP	E_{max}	E_{min}	E_{avg}	E_{sd}
1	1.6100	0.9120	3.7994	1.9492	0.9119	0.0028	8.8401	0.9550	0.9201	0.9145	5.0842	-7.4960	0.0628	1.9486
5	0.5237	0.9862	0.5977	0.7731	0.9861	-0.0008	3.4936	0.9931	0.9867	0.9766	2.9940	-7.6424	-0.0176	0.7731
10	0.3691	0.9938	0.2683	0.5180	0.9938	-0.0005	2.3412	0.9969	0.9939	0.9859	2.7710	-4.0582	-0.0115	0.5180
15	0.2995	0.9961	0.1689	0.4110	0.9961	0.0002	1.8589	0.9980	0.9962	0.9893	2.2076	-2.2004	0.0045	0.4110
20	0.2668	0.9970	0.1283	0.3582	0.9970	0.0004	1.6204	0.9985	0.9971	0.9909	2.0362	-1.6279	0.0094	0.3581
25	0.2218	0.9979	0.0923	0.3037	0.9979	0.0002	1.3739	0.9989	0.9979	0.9925	2.1201	-1.5241	0.0048	0.3038
30	0.2016	0.9981	0.0803	0.2835	0.9981	0.0000	1.2819	0.9991	0.9982	0.9930	1.6001	-2.2739	-0.0007	0.2835
35	0.1846	0.9985	0.0632	0.2515	0.9985	0.0001	1.1374	0.9993	0.9986	0.9939	1.2629	-1.2568	0.0014	0.2515
40	0.1810	0.9985	0.0656	0.2562	0.9985	-0.0001	1.1584	0.9992	0.9985	0.9938	2.3430	-1.1711	-0.0025	0.2562
45	0.1723	0.9987	0.0556	0.2358	0.9987	0.0003	1.0668	0.9994	0.9987	0.9943	1.2056	-1.0210	0.0073	0.2358
50	0.1659	0.9988	0.0509	0.2257	0.9988	-0.0002	1.0204	0.9994	0.9988	0.9946	1.0004	-1.3008	-0.0052	0.2257
55	0.1978	0.9981	0.0829	0.2879	0.9981	-0.0002	1.3019	0.9990	0.9981	0.9929	1.4922	-3.2508	-0.0044	0.2880

60	0.1483	0.9989	0.0467	0.2161	0.9989	0.0002	0.9773	0.9995	0.9990	0.9949	1.2772	-1.3017	0.0042	0.2161
65	0.1425	0.9991	0.0394	0.1984	0.9991	0.0001	0.8973	0.9995	0.9991	0.9953	1.0810	-0.8680	0.0028	0.1984
70	0.1599	0.9988	0.0522	0.2284	0.9988	-0.0002	1.0329	0.9994	0.9988	0.9945	1.1914	-1.4066	-0.0046	0.2285
75	0.1479	0.9989	0.0461	0.2146	0.9989	-0.0003	0.9703	0.9995	0.9990	0.9949	1.7991	-1.1182	-0.0064	0.2146
80	0.1591	0.9989	0.0496	0.2226	0.9989	0.0000	1.0068	0.9994	0.9989	0.9947	1.1238	-1.2733	-0.0005	0.2227
85	0.1652	0.9987	0.0554	0.2355	0.9987	0.0003	1.0652	0.9994	0.9987	0.9944	1.3639	-1.1823	0.0075	0.2354
90	0.1309	0.9991	0.0386	0.1966	0.9991	-0.0001	0.8888	0.9996	0.9991	0.9954	1.3561	-1.4652	-0.0030	0.1966
95	0.1439	0.9988	0.0512	0.2262	0.9988	0.0001	1.0231	0.9994	0.9988	0.9946	2.5161	-1.1762	0.0027	0.2263
100	0.1586	0.9988	0.0532	0.2307	0.9988	0.0002	1.0433	0.9994	0.9988	0.9945	1.6457	-1.5333	0.0039	0.2307
110	0.1581	0.9983	0.0719	0.2681	0.9983	0.0004	1.2131	0.9992	0.9984	0.9935	3.7589	-1.6703	0.0096	0.2680
120	0.1512	0.9988	0.0526	0.2294	0.9988	-0.0001	1.0375	0.9994	0.9988	0.9945	1.6584	-2.0820	-0.0019	0.2295
130	0.1502	0.9988	0.0535	0.2312	0.9988	0.0002	1.0459	0.9994	0.9988	0.9945	1.2606	-2.5799	0.0035	0.2313
140	0.1652	0.9985	0.0634	0.2518	0.9985	0.0005	1.1393	0.9993	0.9986	0.9939	1.3945	-1.8922	0.0121	0.2516
150	0.1476	0.9986	0.0588	0.2426	0.9986	0.0007	1.0977	0.9993	0.9987	0.9942	2.8214	-1.1260	0.0146	0.2422
160	0.1810	0.9983	0.0736	0.2713	0.9983	0.0002	1.2274	0.9991	0.9983	0.9934	2.7794	-1.4415	0.0052	0.2714
170	0.1466	0.9988	0.0523	0.2287	0.9988	0.0001	1.0344	0.9994	0.9988	0.9945	1.3593	-1.2645	0.0018	0.2288
180	0.1738	0.9982	0.0774	0.2782	0.9982	0.0002	1.2583	0.9991	0.9983	0.9932	1.5396	-1.5826	0.0038	0.2782
190	0.1824	0.9978	0.0933	0.3054	0.9978	0.0008	1.3821	0.9989	0.9978	0.9924	3.1199	-2.2100	0.0166	0.3050
200	0.1686	0.9980	0.0876	0.2959	0.9980	-0.0006	1.3375	0.9990	0.9980	0.9927	1.9551	-2.9650	-0.0138	0.2957

Table 10. Accuracy metrics obtained for monthly average daily internal air temperature.

# Neurons	MAE	R^2	MSE	RMSE	EC	CRM	COV	Corr - R	COD	OIMP	E_{max}	E_{min}	E_{avg}	E_{sd}
1	1.1333	0.9446	2.0228	1.4222	0.9446	0.0005	6.3676	0.9719	0.9500	0.9407	4.2588	-4.3123	0.0114	1.4225
5	0.4510	0.9887	0.4125	0.6422	0.9887	-0.0006	2.8722	0.9943	0.9891	0.9801	2.6399	-2.5621	-0.0140	0.6422
10	0.3467	0.9927	0.2678	0.5175	0.9927	-0.0013	2.3127	0.9963	0.9931	0.9849	5.3507	-1.9683	-0.0280	0.5168
15	0.2638	0.9960	0.1472	0.3836	0.9960	-0.0001	1.7165	0.9980	0.9960	0.9895	2.5613	-2.0214	-0.0014	0.3837
20	0.2194	0.9971	0.1053	0.3245	0.9971	0.0000	1.4522	0.9986	0.9972	0.9914	2.1078	-2.1509	-0.0007	0.3246
25	0.1584	0.9983	0.0603	0.2455	0.9983	0.0000	1.0987	0.9992	0.9984	0.9937	2.2747	-2.1199	-0.0005	0.2456
30	0.1645	0.9983	0.0616	0.2481	0.9983	0.0000	1.1102	0.9992	0.9983	0.9937	1.8305	-2.1507	-0.0008	0.2482
35	0.1420	0.9988	0.0430	0.2074	0.9988	-0.0002	0.9279	0.9994	0.9988	0.9948	1.8380	-1.8844	-0.0053	0.2074
40	0.1423	0.9987	0.0482	0.2196	0.9987	0.0000	0.9825	0.9993	0.9987	0.9945	2.2282	-1.4381	-0.0006	0.2196
45	0.1295	0.9990	0.0374	0.1933	0.9990	0.0003	0.8651	0.9995	0.9990	0.9952	1.6846	-1.5782	0.0062	0.1932
50	0.1267	0.9990	0.0377	0.1943	0.9990	0.0000	0.8693	0.9995	0.9990	0.9952	2.1834	-1.4136	-0.0010	0.1943
55	0.1714	0.9979	0.0775	0.2784	0.9979	-0.0004	1.2455	0.9989	0.9979	0.9928	2.1031	-3.5315	-0.0093	0.2784
60	0.1124	0.9992	0.0293	0.1711	0.9992	0.0005	0.7662	0.9996	0.9992	0.9958	1.6089	-1.4947	0.0104	0.1709
65	0.1048	0.9993	0.0260	0.1613	0.9993	0.0003	0.7220	0.9996	0.9993	0.9961	1.6623	-1.3956	0.0072	0.1612
70	0.1235	0.9991	0.0345	0.1856	0.9991	0.0002	0.8308	0.9995	0.9991	0.9954	1.6529	-1.4216	0.0049	0.1856
75	0.1097	0.9992	0.0310	0.1759	0.9992	0.0001	0.7873	0.9996	0.9992	0.9957	1.4127	-1.5945	0.0015	0.1760
80	0.1389	0.9988	0.0454	0.2130	0.9988	0.0001	0.9532	0.9994	0.9988	0.9947	1.7571	-1.6012	0.0015	0.2130
85	0.1305	0.9987	0.0460	0.2145	0.9987	0.0005	0.9602	0.9994	0.9988	0.9946	1.6732	-2.1620	0.0121	0.2142
90	0.0958	0.9993	0.0262	0.1619	0.9993	-0.0002	0.7243	0.9996	0.9993	0.9960	1.5787	-1.6375	-0.0042	0.1619
95	0.1110	0.9989	0.0394	0.1986	0.9989	0.0000	0.8887	0.9995	0.9989	0.9951	2.5585	-1.5243	0.0006	0.1986
100	0.1324	0.9988	0.0443	0.2104	0.9988	0.0002	0.9415	0.9994	0.9988	0.9947	1.7455	-1.4408	0.0038	0.2104
110	0.1312	0.9988	0.0429	0.2071	0.9988	0.0005	0.9271	0.9994	0.9988	0.9948	2.1811	-1.0168	0.0102	0.2069
120	0.1203	0.9989	0.0385	0.1962	0.9989	0.0001	0.8779	0.9995	0.9990	0.9951	1.2322	-1.8728	0.0029	0.1962
130	0.1224	0.9991	0.0344	0.1854	0.9991	0.0001	0.8296	0.9995	0.9991	0.9954	1.5293	-0.8919	0.0020	0.1854
140	0.1295	0.9987	0.0463	0.2151	0.9987	0.0005	0.9633	0.9994	0.9987	0.9946	1.6267	-1.2653	0.0119	0.2149
150	0.1178	0.9988	0.0445	0.2109	0.9988	0.0007	0.9446	0.9994	0.9989	0.9947	2.8318	-1.1689	0.0151	0.2104
160	0.1498	0.9984	0.0594	0.2438	0.9984	0.0011	1.0921	0.9992	0.9984	0.9938	2.2428	-1.3623	0.0242	0.2426
170	0.1251	0.9989	0.0414	0.2034	0.9989	-0.0004	0.9099	0.9994	0.9989	0.9949	1.2108	-1.6322	-0.0081	0.2033
180	0.1633	0.9980	0.0735	0.2711	0.9980	0.0003	1.2136	0.9990	0.9980	0.9930	1.7961	-1.4238	0.0058	0.2711
190	0.1675	0.9980	0.0726	0.2694	0.9980	-0.0004	1.2051	0.9990	0.9981	0.9930	2.1408	-1.6623	-0.0082	0.2693
200	0.1417	0.9984	0.0594	0.2437	0.9984	-0.0005	1.0900	0.9992	0.9984	0.9938	1.4616	-1.8702	-0.0111	0.2435

Table 11. Accuracy metrics obtained for monthly average daily values of all outputs (optimal values in bold).

# Neurons	MAE	R^2	MSE	RMSE	EC	CRM	COV	Corr - R	COD	OIMP	E_{max}	E_{min}	E_{avg}	E_{sd}
1	1.2956	0.9319	2.6377	1.6241	0.9319	0.001358	7.3063	0.9653	0.9383	0.9314	5.0842	-7.4960	0.0302	1.6239
5	0.4813	0.9867	0.5158	0.7182	0.9867	-0.000689	3.2245	0.9933	0.9873	0.9781	2.9940	-7.6856	-0.0153	0.7181
10	0.3481	0.9935	0.2517	0.5017	0.9935	-0.000877	2.2521	0.9967	0.9937	0.9861	5.3507	-4.5244	-0.0195	0.5014
15	0.2726	0.9962	0.1477	0.3843	0.9962	0.000034	1.7266	0.9981	0.9963	0.9899	2.5613	-2.2004	0.0008	0.3843
20	0.2319	0.9973	0.1060	0.3256	0.9973	0.000183	1.4631	0.9986	0.9973	0.9917	2.1078	-2.1509	0.0041	0.3256
25	0.1783	0.9982	0.0680	0.2607	0.9982	0.000083	1.1715	0.9991	0.9983	0.9936	2.2747	-2.1199	0.0018	0.2608

30	0.1750	0.9983	0.0649	0.2547	0.9983	-0.000083	1.1443	0.9992	0.9984	0.9937	1.8305	-2.2739	-0.0018	0.2547
35	0.1549	0.9988	0.0471	0.2170	0.9988	-0.000109	0.9750	0.9994	0.9988	0.9948	1.8380	-1.8844	-0.0024	0.2171
40	0.1529	0.9987	0.0510	0.2258	0.9987	-0.000035	1.0146	0.9993	0.9987	0.9945	2.3430	-1.4381	-0.0008	0.2259
45	0.1428	0.9989	0.0415	0.2038	0.9989	0.000303	0.9158	0.9995	0.9989	0.9951	1.6846	-1.5782	0.0067	0.2037
50	0.1376	0.9990	0.0393	0.1981	0.9990	-0.000210	0.8900	0.9995	0.9990	0.9953	2.1834	-1.4555	-0.0047	0.1981
55	0.1757	0.9981	0.0737	0.2715	0.9981	-0.000281	1.2194	0.9990	0.9981	0.9933	2.1031	-3.5315	-0.0063	0.2714
60	0.1231	0.9991	0.0334	0.1828	0.9991	0.000385	0.8214	0.9996	0.9992	0.9957	1.6089	-1.4947	0.0086	0.1826
65	0.1169	0.9992	0.0292	0.1709	0.9992	0.000225	0.7680	0.9996	0.9993	0.9960	1.6623	-1.3956	0.0050	0.1709
70	0.1335	0.9990	0.0382	0.1955	0.9990	0.000040	0.8784	0.9995	0.9990	0.9953	1.6529	-1.4216	0.0009	0.1955
75	0.1211	0.9991	0.0345	0.1858	0.9991	-0.000042	0.8347	0.9996	0.9991	0.9956	1.7991	-1.5945	-0.0009	0.1858
80	0.1419	0.9989	0.0438	0.2092	0.9989	**0.000005**	0.9398	0.9994	0.9989	0.9950	1.7571	-1.7636	**0.0001**	0.2092
85	0.1409	0.9988	0.0467	0.2161	0.9988	0.000491	0.9711	0.9994	0.9988	0.9948	1.6732	-2.1620	0.0109	0.2158
90	**0.1065**	**0.9993**	**0.0289**	**0.1699**	**0.9993**	-0.000168	**0.7631**	**0.9996**	**0.9993**	**0.9960**	1.5787	-1.6375	-0.0037	**0.1699**
95	0.1204	0.9989	0.0416	0.2039	0.9989	0.000071	0.9160	0.9995	0.9989	0.9951	2.5874	-1.5243	0.0016	0.2039
100	0.1386	0.9988	0.0448	0.2116	0.9988	0.000277	0.9511	0.9994	0.9989	0.9949	1.7455	-1.5333	0.0062	0.2116
110	0.1398	0.9985	0.0564	0.2374	0.9985	0.000468	1.0670	0.9993	0.9986	0.9942	3.7589	-1.6703	0.0104	0.2372
120	0.1295	0.9989	0.0428	0.2070	0.9989	0.000061	0.9300	0.9994	0.9989	0.9950	2.0648	-2.0820	0.0014	0.2070
130	0.1329	0.9989	0.0424	0.2059	0.9989	0.000122	0.9251	0.9995	0.9989	0.9951	1.5293	-2.5817	0.0027	0.2059
140	0.1396	0.9987	0.0505	0.2247	0.9987	0.000503	1.0101	0.9993	0.9987	0.9946	1.8538	-1.8922	0.0112	0.2245
150	0.1278	0.9987	0.0496	0.2228	0.9987	0.000629	1.0015	0.9994	0.9988	0.9946	2.9497	**-1.2934**	0.0140	0.2224
160	0.1601	0.9984	0.0633	0.2517	0.9984	0.000507	1.1312	0.9992	0.9984	0.9938	2.7794	-1.4415	0.0113	0.2514
170	0.1310	0.9989	0.0433	0.2081	0.9989	-0.000014	0.9349	0.9994	0.9989	0.9950	**1.3593**	-1.6322	-0.0003	0.2081
180	0.1637	0.9981	0.0723	0.2689	0.9981	0.000316	1.2083	0.9991	0.9982	0.9933	1.7961	-1.5826	0.0070	0.2688
190	0.1715	0.9979	0.0808	0.2842	0.9979	0.000233	1.2771	0.9990	0.9980	0.9929	3.1199	-2.2985	0.0052	0.2842
200	0.1534	0.9981	0.0724	0.2690	0.9981	-0.000512	1.2079	0.9991	0.9982	0.9933	1.9779	-2.9650	-0.0114	0.2688

In particular, the comparison between the tables shows that the ANN has a lower prediction capacity for external surface temperature than the other two because, when considering the same number of neurons, worse index values are shown.

In order to determine the ideal number of neurons in the hidden layer, the optimal statistical indices related to the overall case taking into account all three temperature quantities were examined.

From the Table 11, it is highlighted that the trends of the mean square error (MSE), the mean absolute error (MAE) and the root mean square error (RMSE) decrease as the number of neurons in the hidden layer increases, reaching the minimum in the configuration characterized by 90 neurons. The minimum values are 0.0289, 0.1065 and 0.1699, respectively. From 90 neurons onwards the trends increase and decrease in a not very relevant way. Moreover, a trend of the coefficient of residual mass (CRM) extremely variable in a random way, between 0.0014 and -0.0009, is noticed demonstrating that, globally, the ANN can overestimate or underestimate the target values by modifying the number of neurons.

It is also shown that the trends of the R-square (R^2), efficiency coefficient (EC), correlation coefficient (CC), determination coefficient (COD) and a general index of model performance (OIMP) grow as the number of neurons in the hidden layer increases, reaching a maximum in the configuration with 90 neurons. The maximum values are very close to unity and are equal, respectively, to 0.9993, 0.9993, 0.9996, 0.9993 and 0.9960. Also in this case, starting from 90 neurons the trends increase and decrease in an insignificant way.

Definitively, Table 11 shows how the lowest values, close to zero, of the MAE, MSE, RMSE, COV, CRM, and E_{sd} indices, and the highest values, close to unity, of R, R^2, EC, COD, and OIMP were obtained for ANN with 90 neurons in the hidden layer. It is also noted that the minimum value for the maximum, minimum, mean and standard deviation error is not obtained for this configuration.

This allowed us to notice that the optimal architecture of ANN is the one with 90 neurons in the hidden layer since most of the metrics of optimal accuracy fall in such configuration.

The minimum value of E_{max}, E_{min}, and E_m are obtained for 170, 150, and 80 neurons in the hidden layer, respectively.

In addition, the E_i errors, committed by the ANN in the training phase in obtaining the target values, were also used to draw the overall box plot, shown in Figure 11.

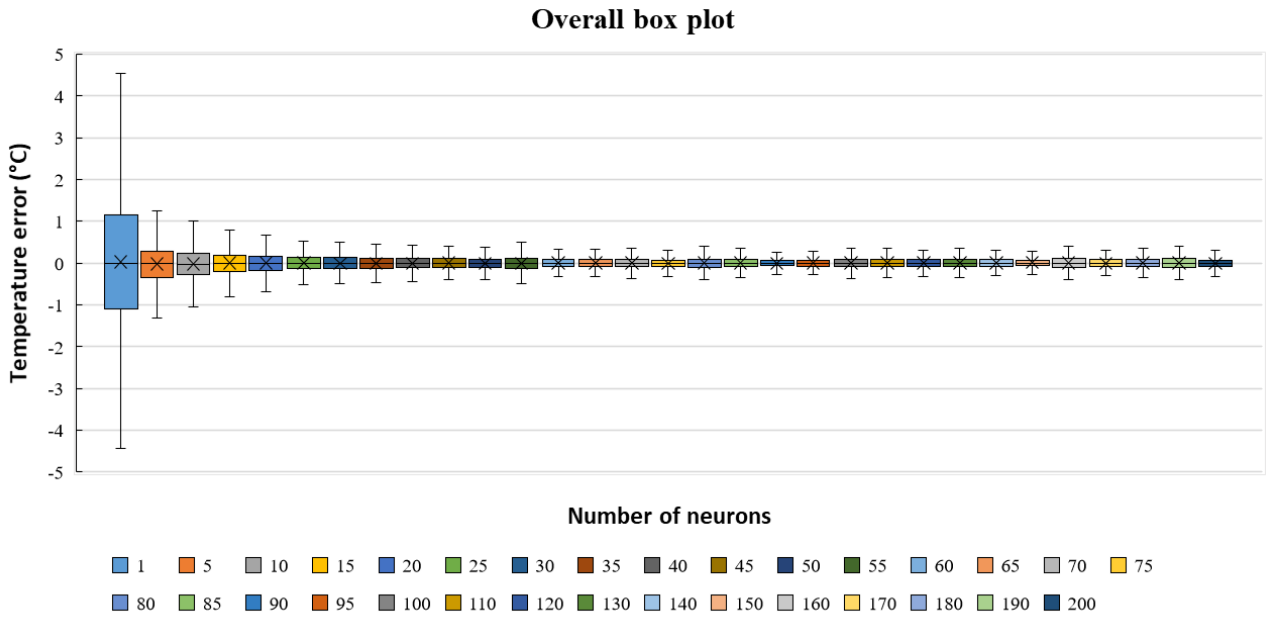

Figure 11. Overall box plot of errors committed by the ANN in the training phase in obtaining the target values.

It can be seen from the figure that the error box plot suffers a reduction in its interquartile range (the difference between the third and first quartiles), median, and whisker size by using a large number of neurons in the hidden layer.
Finally, the trends of the number of iterations and time used, as well as the trend of the time needed per iteration, by varying the number of neurons in the hidden layer, were reported in Figure 12 to understand the computational burden related to each ANN configuration.

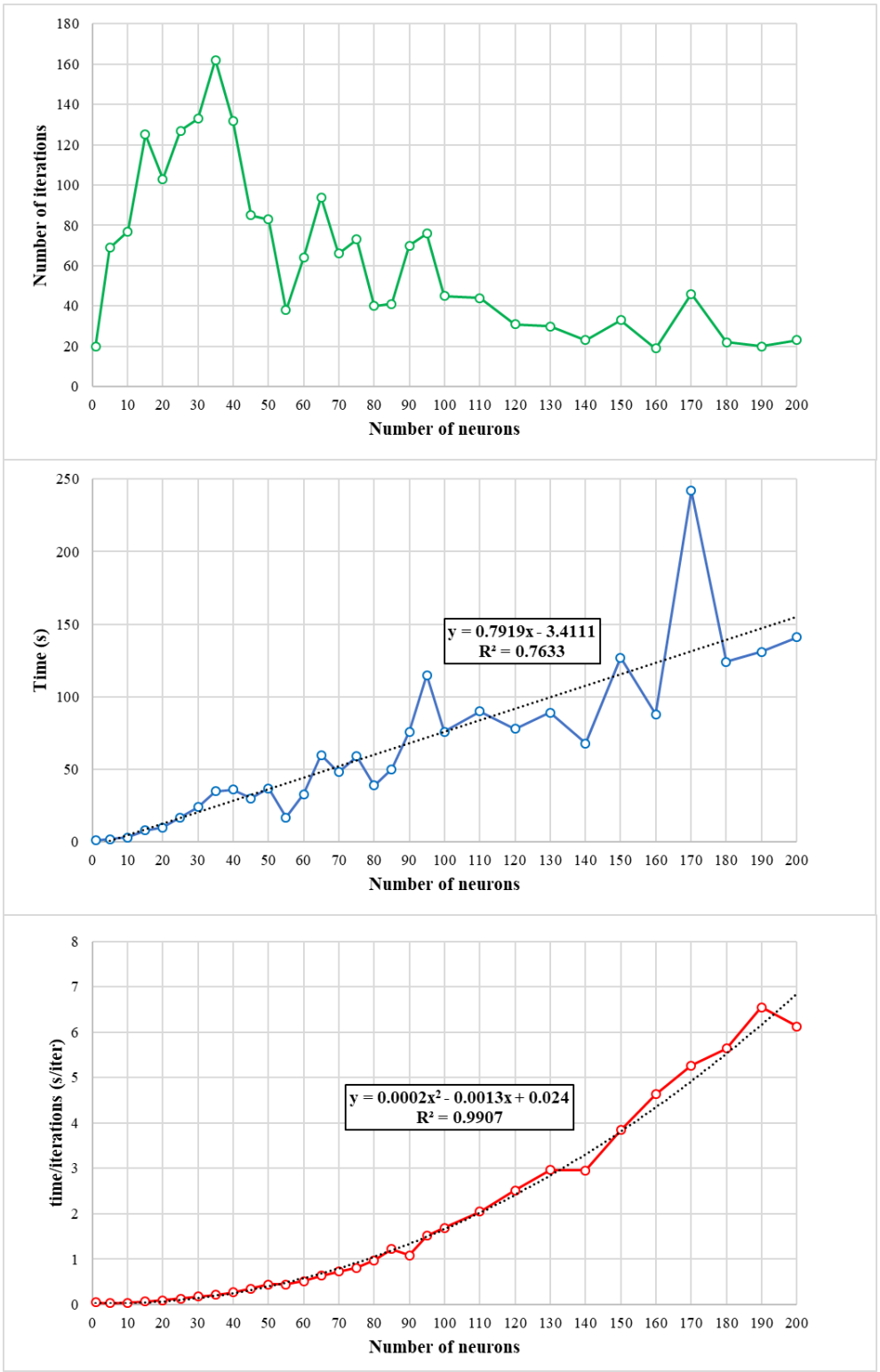

Figure 12. Trends of the number of iterations, time used and time needed per iteration by varying the number of neurons in the hidden layer

The figure shows how the trend of the number of iterations employed in every single process of training is quite variable from 1 to 100 neurons while from 100 to 200 neurons a decreasing trend is noticed; therefore as the complexity of the network increases the iterations decrease. The trend of the time employed in each process of the ANN training is rather increasing, that is, as the number of neurons in the hidden layer increases, the time required increases. Finally, for greater clarity, the trend

of the time used for each iteration has been graphically shown, which has an increasing behaviour in relation to an equation of second degree.
The ANN optimal configuration, obtained from the analysis of the training phase, is characterized by 90 neurons in the hidden layer. The training process of the ANN ended after 86 seconds and 70 iterations and is stopped with a gradient value of 0.13791 and a value of the damping parameter μ of 1×10^{-5}.
Figure 13 shows some characteristics of the optimal ANN architecture, such as the box plots of the errors for all three temperatures, both separately and overall.

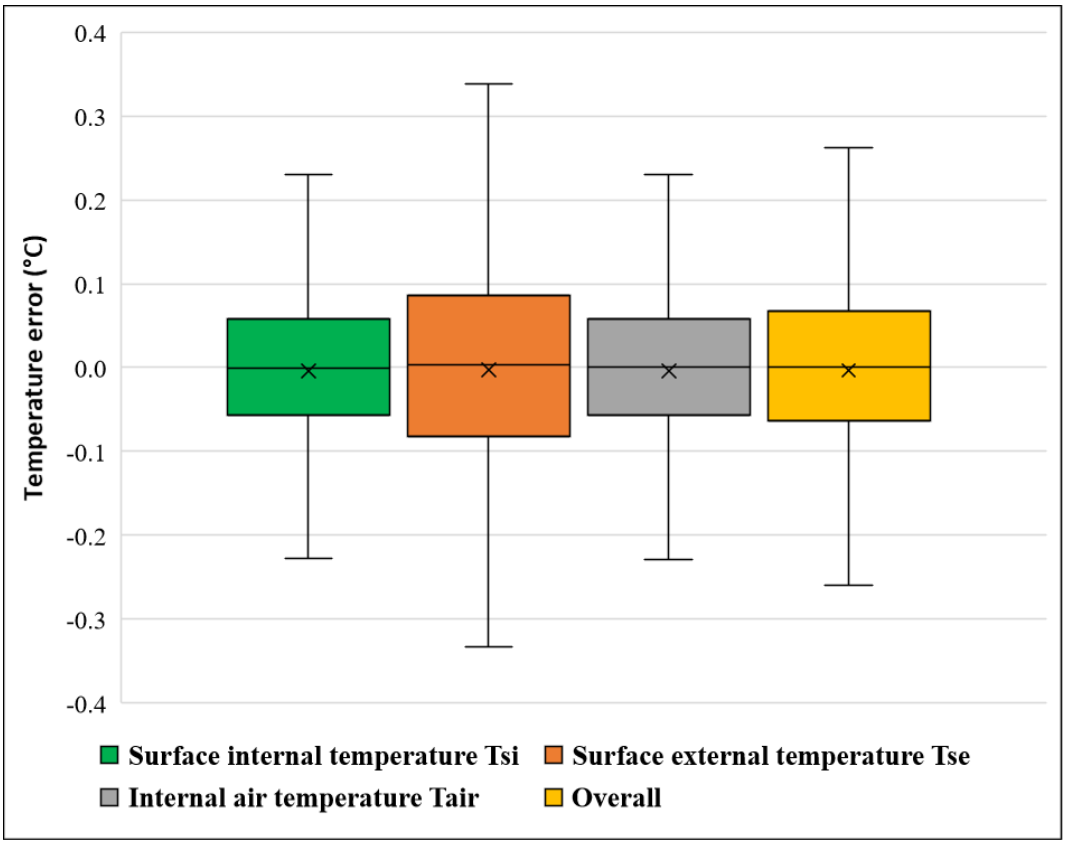

Figure 13. Box plots of the optimal ANN errors

From Figure 13, it is evident that the box plots of the errors are completely concentrated around zero. The error associated with the internal surface temperature varies between -0.0564 and 0.0584; the one related to the external surface temperature varies between -0.0825 and 0.0858; the one related to the internal air temperature varies between -0.0569 and 0.0581; while the overall error, which takes into account all three quantities, varies between -0.0640 and 0.0667.
In addition, the Regression plot of optimal ANN and target temperatures considering single and all outputs simultaneously are shown in Figure 14.

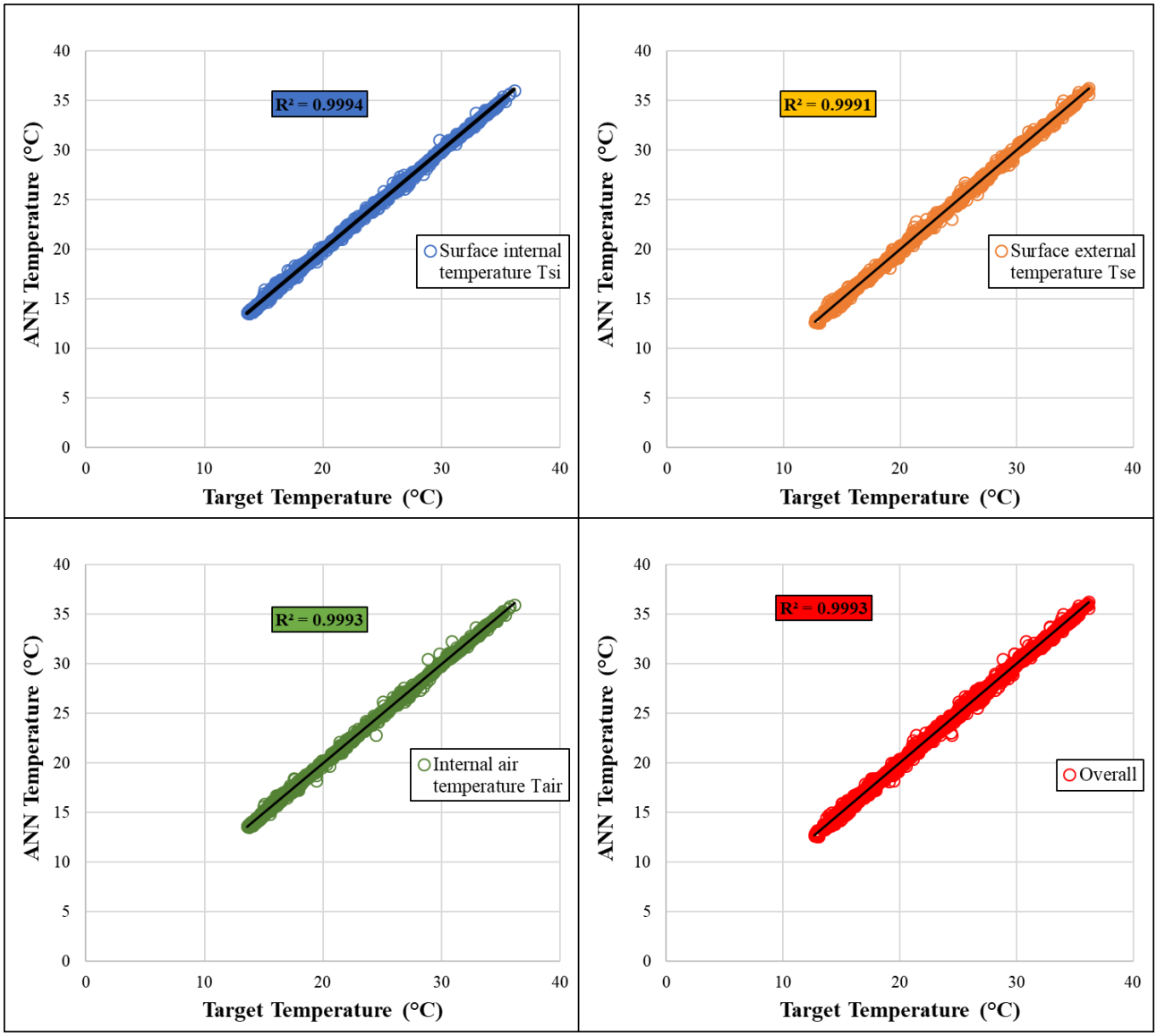

Figure 14. Regression plot of optimal ANN and target temperatures considering single and all outputs simultaneously.

From Figure 14, it is easy to detect how there is a high correlation between the outputs obtained from the application of the optimal ANN and the targets simulated with the software Design Builder so much so that all the data result overlapped and almost concentrated in the bisector, both for the single cases and for the total. The graph also shows the R^2 coefficient, which is very close to unity in each case.

By considering the yearly average temperature as the representative temperature of 36 green roofs considered for each substrate type, further analysis has demonstrated that there is a perfect correspondence between the ANN temperatures and the target temperatures, for all three temperatures considered. The results of this comparative analysis are reported in the supplementary file. In the same Supplementary file, the Matlab script of the optimal ANN architecture is available.

3.1.2. Impact of the number of hidden layers

The successive step aims to identify the best number of hidden layers that maximize the ANN accuracy. For this reason, the 90 neurons found as optimal in the previous analysis were distributed

into one, two and three hidden layers, as shown in Figure 15, and the accuracy metrics were calculated as well.

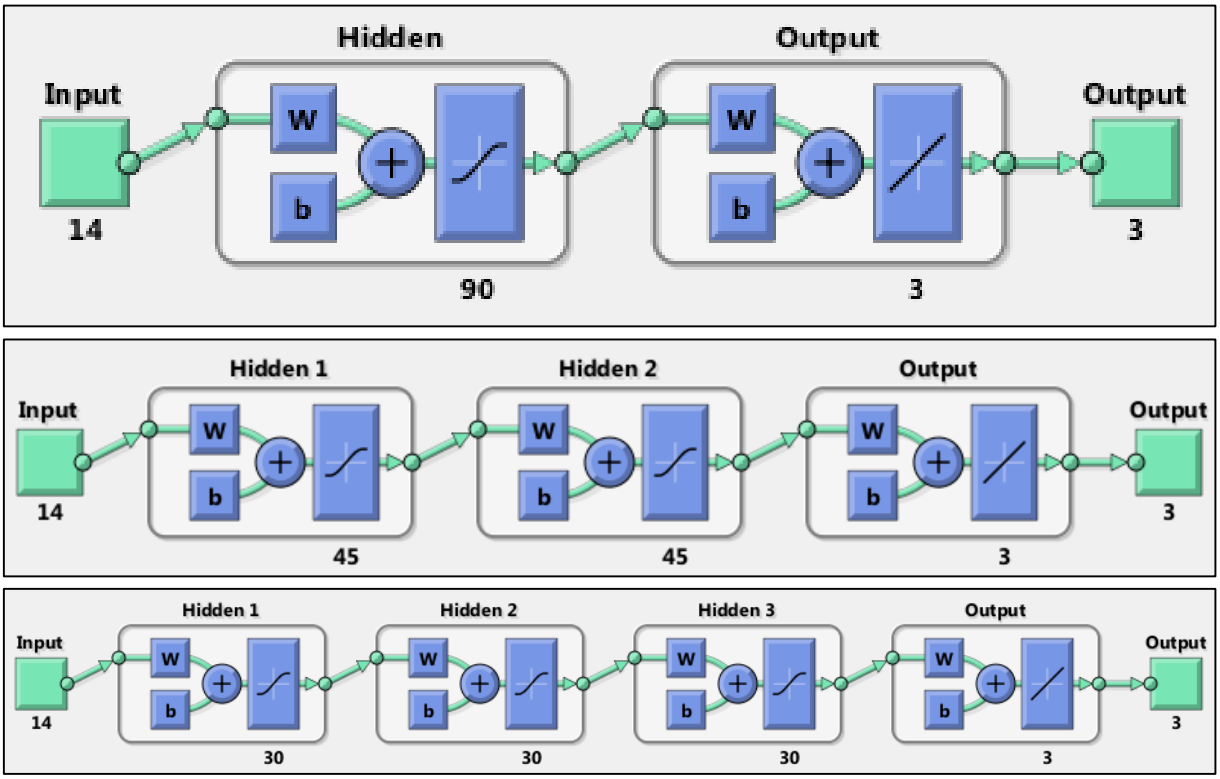

Figure 15. ANN with 90 neurons in one, two and three hidden layers.

Table 12 lists the accuracy metrics for both the individual outputs and the overall case, at a daily average monthly level, in order to ascertain what is the optimal number of hidden levels, given a certain number of neurons, equal to 90 in this case.

Table 12. Values of accuracy metrics as the number of hidden levels changes for monthly average daily internal and external surface temperature, internal air temperature and overall.

	Tsi (°C)			Tse (°C)			Tair (°C)			Overall		
# Hidden layer	**1**	**2**	**3**	**1**	**2**	**3**	**1**	**2**	**3**	**1**	**2**	**3**
MAE	0.093	0.149	0.137	0.131	0.189	0.177	0.096	0.154	0.139	0.106	0.164	0.151
R^2	0.999	0.998	0.998	0.999	0.998	0.998	0.999	0.998	0.998	0.999	0.998	0.998
MSE	0.022	0.076	0.068	0.039	0.095	0.093	0.026	0.078	0.073	0.029	0.083	0.078
RMSE	0.147	0.276	0.262	0.197	0.308	0.305	0.162	0.280	0.271	0.170	0.288	0.280
EC	0.999	0.998	0.998	0.999	0.998	0.998	0.999	0.998	0.998	0.999	0.998	0.998
CRM	0.000	0.000	0.001	0.000	0.001	0.001	0.000	0.001	0.001	0.000	0.001	0.001
COV	0.661	1.237	1.173	0.889	1.394	1.380	0.724	1.254	1.212	0.763	1.296	1.257
Corr	1.000	0.999	0.999	1.000	0.999	0.999	1.000	0.999	0.999	1.000	0.999	0.999
COD	0.999	0.998	0.998	0.999	0.998	0.998	0.999	0.998	0.998	0.999	0.998	0.998
OIMP	0.996	0.993	0.993	0.995	0.992	0.992	0.996	0.993	0.993	0.996	0.993	0.993
Emax	0.817	2.418	4.123	1.356	2.116	5.430	1.579	2.383	4.141	1.579	2.418	5.430
Emin	-1.203	-1.680	-1.673	-1.465	-1.995	-1.894	-1.638	-1.685	-1.671	-1.638	-1.995	-1.894
Eavg	-0.004	0.010	0.025	-0.003	0.019	0.031	-0.004	0.019	0.021	-0.004	0.016	0.026
Esd	0.147	0.276	0.260	0.197	0.307	0.303	0.162	0.279	0.270	0.170	0.288	0.278

It can be seen, both for the single outputs and overall case, that there is an increasing trend in the maximum error (E_{max}) and the average error (E_{avg}) as the number of hidden layers increases. As far as the coefficient of variance (COV), the minimum error (E_{min}) and the standard deviation of the error (E_{sd}) are concerned, there is an upward trend from one to two hidden layers and a slight downward trend from two to three hidden layers.
From the same table, it is detected that the highest values of the mean square error (MSE), the mean absolute error (MAE) and the root mean square error (RMSE) are recorded for the case with two hidden layers, while the lowest values of these quantities occur for the case of a single hidden layer. Therefore, the configuration characterized by 90 neurons divided into 3 hidden layers turns out to be the intermediate one. Furthermore, it can be seen that there is a trend of the residual mass coefficient (CRM) increasing as the number of hidden layers increases.
Finally, the R-square (R^2), the efficiency coefficient (EC), the correlation coefficient (CC), the determination coefficient (COD), and the general index of model performance (OIMP) in going from the case with one layer to the case with two hidden layers decrease, while they undergo a slight increase in the case with three hidden layers.
Therefore, it can be deduced that the best accuracy metrics are obtained in the configuration with a single hidden layer consisting of 90 neurons which thus represents the one proposed as optimal in this research work.

3.2. Validation of the ANN for different green roofs

The next step after the training phase aimed to validate the optimized ANN to evaluate its accuracy in the determination of the thermal impact of green roofs not falling in the configurations used to train it. In particular, the ANN was validated for the two remaining cases of vegetated roof configurations with a different substrate layer not used in the training phase, as indicated in Section 2.1.3. They were simulated with the software Design Builder to predict the outputs related to the three temperatures.
In order to calculate the internal surface, external surface and internal air temperatures for the remaining substrates not used in the training phase, the optimal configuration of ANN with 90 neurons in the hidden layer was used.
For each soil a "validation parametric table" was created, to be given as input to the optimal neural network constituted, by a number of columns equal to the inputs considered, similar to those of the training phase, and by a number of rows equal to the product between the 36 configurations of green roof containing the specific substrate considered and the number of months of the year. Therefore, this parametric validation table, for a specific soil substrate, consists of 14 columns (14 inputs, see Table 6) and 432 rows. Altogether, for the two substrates, 864 monthly green roof thermal performances are to be validated. The Matlab script, reported in the Supplementary file was used to predict the monthly average daily thermal performance of the green roof.
Figures 16 and 17 show the regression curves related to the comparison between the ANN outputs and target outputs, respectively for the substrates 3 and 6 by considering the single outputs and overall.

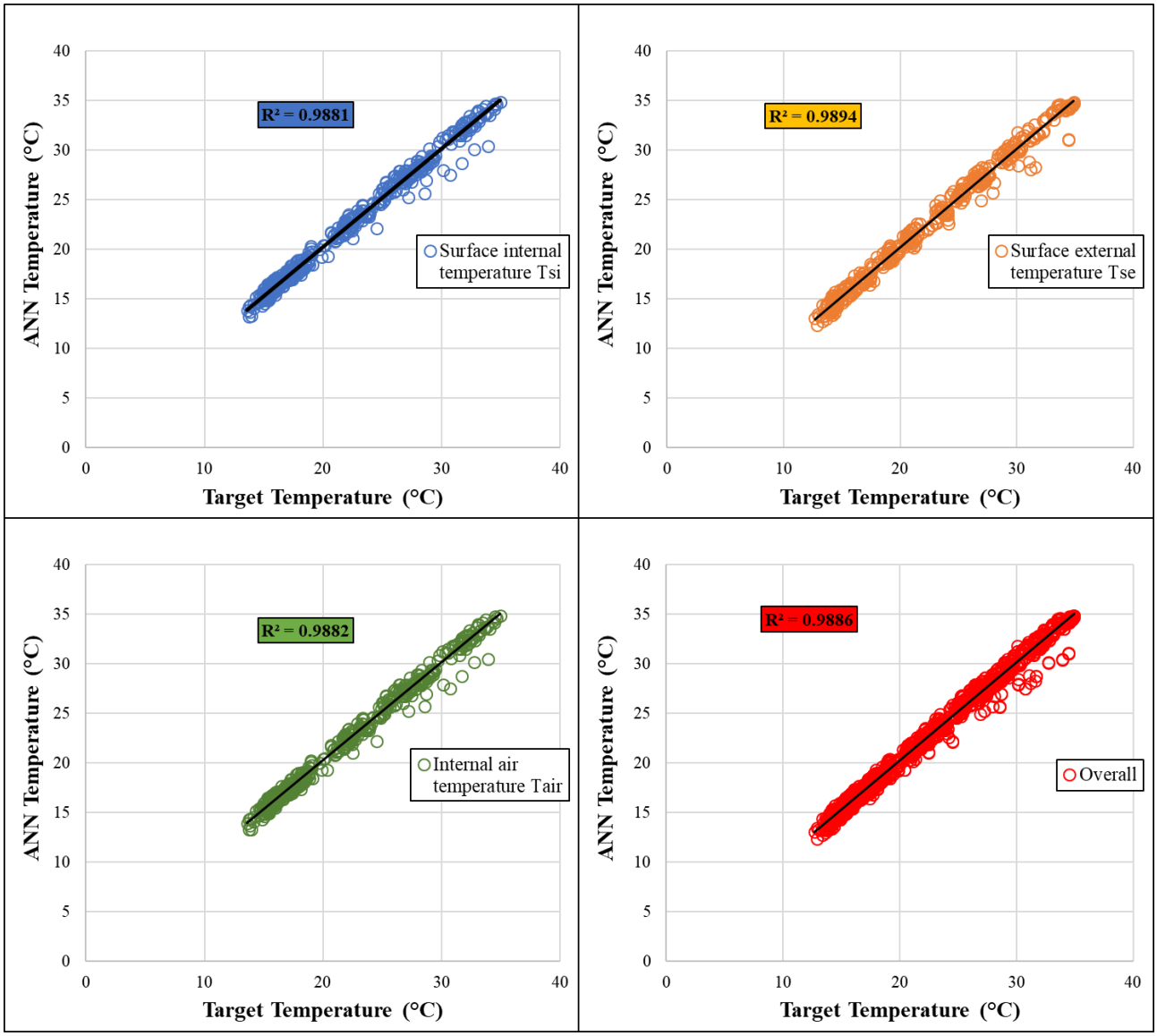

Figure 16. Regression curves related to the comparison between the ANN outputs and target outputs, respectively for the substrate 3 by considering the single and overall outputs.

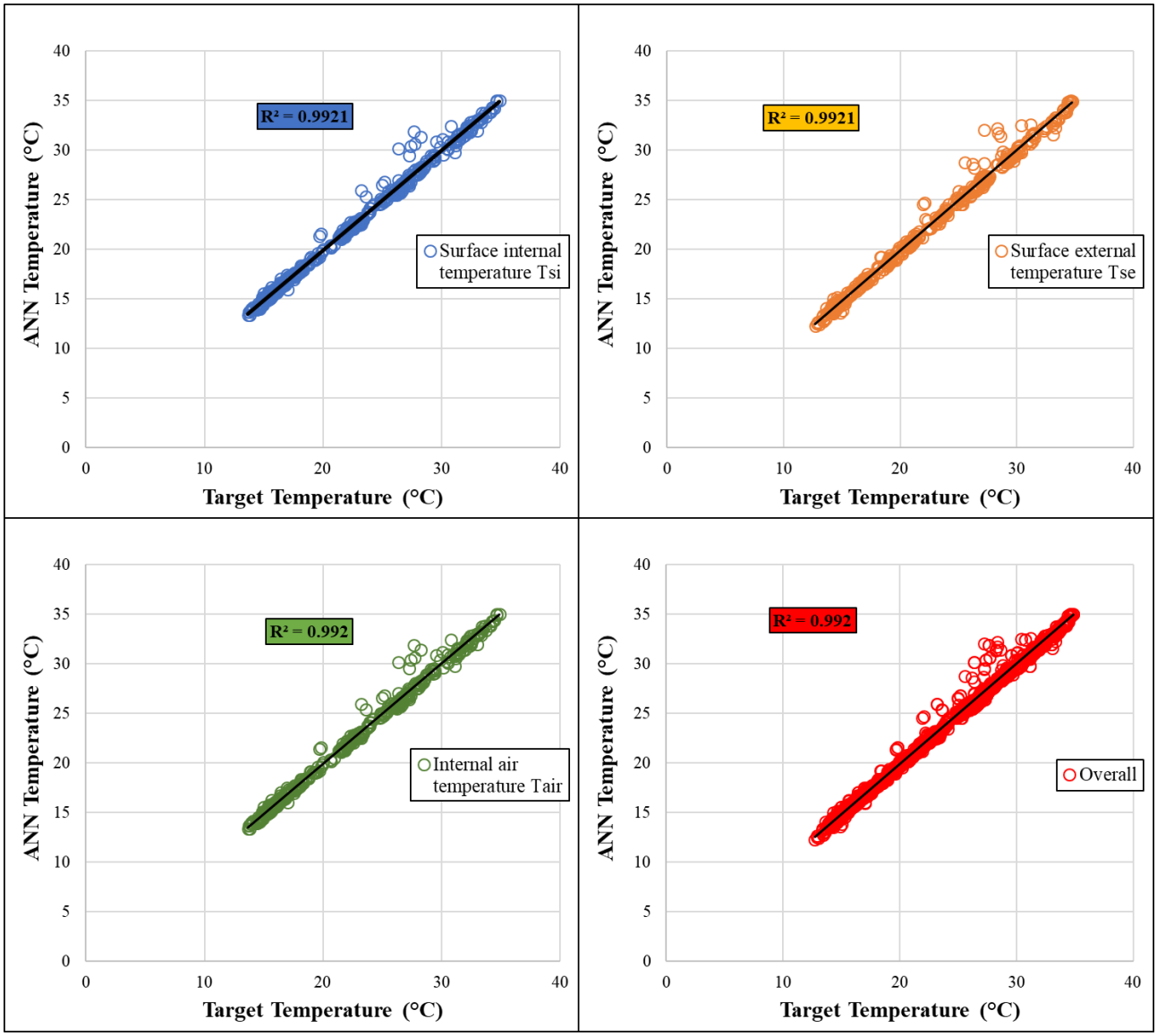

Figure 17. Regression curves related to the comparison between the ANN outputs and target outputs, respectively for the substrate 6 by considering the single outputs and overall.

For both substrates and all outputs, the regression curves are very close to the bisector with a very high R^2, highlighting the very high accuracy of the ANN proposed. Another view of the high accuracy of the ANN can be observed in Figure 18, containing the error boxplots, for the two substrates and different outputs.

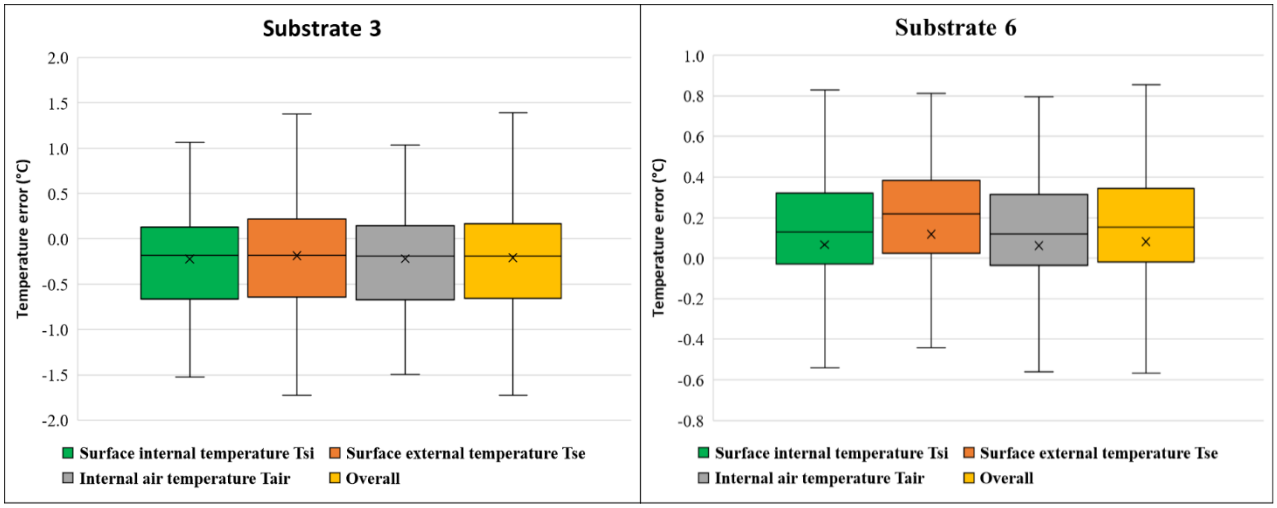

Figure 18. Box plots of output errors. Left: substrate 3; Right: substrate 6

The box plots highlight the error variation range that can be identified by means of the average error, the distribution of the error around the average value with higher frequency, and the maximum and minimum errors observed with lower frequency. The values of the average error, for substrate 3, for the internal surface, external surface and internal air temperatures are -0.221 °C, -0.187 °C and -0.219 °C, respectively. Instead, for substrate 6, the values are 0.066 °C, 0.119 °C and 0.061 °C.

The values of the error standard deviation, for substrate 3, for the internal surface, external surface and internal air temperatures are 0.651 °C, 0.672 °C and 0.649 °C, respectively. Instead, for substrate 6, the values are 0.545 °C, 0.586 °C and 0.547 °C. If all temperature outputs are considered simultaneously the average error and the error standard deviation are, respectively, -0.209 °C and 0.657 °C for substrate 3, and 0.082 °C and 0.560 °C, for substrate 6.

Consequently, the ANN is more accurate to predict the thermal performance of green roofs with heavyweight substrates.

4. Conclusions

The objective of this research work was to develop a dynamic simulation model of the thermal performance of a green roof using ANNs. In doing so, a contribution to the scientific literature was provided in covering the current gap related to the limited application of ANN in the field of green roof thermal performance.

The ANN algorithm proposed in this research work can be used as a simple and alternative tool to simulation software for predicting the green roof thermal performance. In particular, the ANN proposed here is capable to predict monthly values of the external and internal surface temperatures and the air temperature inside an environment. These temperatures are very useful to identify the impact of a green roof on energy loads, indoor thermal comfort, and also the mitigation of the urban heat island.

The ANN was trained by considering several green roof configurations (different vegetation types, different lightweight and heavyweight substrates and different substrates thicknesses) located in Palermo, a city with a Mediterranean climate. Different ANN architectures were considered by varying the number of neurons and hidden layers. The optimal architecture found consists of one hidden layer with 90 neurons.

Results of the validation phase highlighted the high accuracy of such a tool to forecast temperatures for green roofs not considered in the training phase, in comparison with results obtained with dynamical simulation software DesignBuilder.
Among the advantages of the tool proposed, contrary to DesignBuilder, the ANN tool does not require advanced expertise, high computational costs, or a high number of data inputs; it is simple and quick to be used and provides almost the same results, which are the monthly summary of the hourly results. Future improvements of the algorithm created will be conferred by amplifying the training dataset with also other weather conditions. The authors are currently developing such research extensions. Anyway, this is a useful tool for an expert in this field to simulate the thermal green roof performance in Mediterranean climates, very similar to those of Palermo.

References

[1] M. Manso, I. Teotónio, C. M. Silva, C. O. Cruz, Green roof and green wall benefits and costs: A review of the quantitative evidence, Renewable and Sustainable Energy Reviews, Volume 135, 2021, 110111, ISSN 1364-0321, https://doi.org/10.1016/j.rser.2020.110111.

[2] M. R. Ismail, Quiet environment: Acoustics of vertical green wall systems of the Islamic urban form, Frontiers of Architectural Research, Volume 2, Issue 2, 2013, Pages 162-177, ISSN 2095-2635, https://doi.org/10.1016/j.foar.2013.02.002.

[3] T. Van Renterghem, D. Botteldooren, Reducing the acoustical façade load from road traffic with green roofs, Building and Environment, Volume 44, Issue 5, 2009, Pages 1081-1087, ISSN 0360-1323, https://doi.org/10.1016/j.buildenv.2008.07.013.

[4] D. Lunain, D. Ecotiere, Benoit Gauvreau. In-situ evaluation of the acoustic eff iciency of a green wall in urban area, Internoise 2016, 45th International Congress and Exposition of Noise Control Engineering, Aug 2016, HAMBOURG, Germany. pp. 6592-6601.

[5] S. S. G. Hashemi, H. B.Mahmud, M. A. Ashraf, Performance of green roofs with respect to water quality and reduction of energy consumption in tropics: A review, Renewable and Sustainable Energy Reviews, Volume 52, 2015, Pages 669-679, ISSN 1364-0321, https://doi.org/10.1016/j.rser.2015.07.163.

[6] D. Bradley Rowe, Green roofs as a means of pollution abatement, Environmental Pollution, Volume 159, Issues 8–9, 2011, Pages 2100-2110, ISSN 0269-7491, https://doi.org/10.1016/j.envpol.2010.10.029.

[7] O. Saadatian, K. Sopian, E. Salleh, C.H. Lim, S. Riffat, E. Saadatian, A. Toudeshki, M.Y. Sulaiman, A review of energy aspects of green roofs, Renewable and Sustainable Energy Reviews, Volume 23, 2013, Pages 155-168, ISSN 1364-0321, https://doi.org/10.1016/j.rser.2013.02.022.

[8] C. Lamnatou, D. Chemisana, A critical analysis of factors affecting photovoltaic-green roof performance, Renewable and Sustainable Energy Reviews, Volume 43, 2015, Pages 264-280, ISSN 1364-0321, https://doi.org/10.1016/j.rser.2014.11.048.

[9] B. Y. Schindler, L. Blank, S. Levy, G. Kadas, D. Pearlmutter, L. Blaustein, Integration of photovoltaic panels and green roofs: review and predictions of effects on electricity production and plant communities, Israel Journal of Ecology & Evolution, Volume 62, Issue 1-2, 2016, Pages 68-73, ISSN: 1565-9801, https://doi.org/10.1080/15659801.2015.1048617.

[10] X. Qin, X. Wu, Y.-M. Chiew, Y. Li, A Green Roof Test Bed for Stormwater Management and Reduction of Urban Heat Island Effect in Singapore, International Journal of Environment and Climate Change, Volume 2, Issue 4, 2013, Pages 410-420. https://doi.org/10.9734/BJECC/2012/2704.

[11] M. Santamouris, Cooling the cities – A review of reflective and green roof mitigation technologies to fight heat island and improve comfort in urban environments, Solar Energy, Volume 103, 2014, Pages 682-703, ISSN 0038-092X, https://doi.org/10.1016/j.solener.2012.07.003.
[12] S. S. Alcazar, F. Olivieri, J. Neila, Green roofs: Experimental and analytical study of its potential for urban microclimate regulation in Mediterranean–continental climates, Urban Climate, Volume 17, 2016, Pages 304-317, ISSN 2212-0955, https://doi.org/10.1016/j.uclim.2016.02.004.
[13] F. O. Robbiati, N. Cáceres, E.C. Hick, M. Suarez, S. Soto, G. Barea, E. Matoff, L. Galetto, L. Imhof, Vegetative and thermal performance of an extensive vegetated roof located in the urban heat island of a semiarid region, Building and Environment, Volume 212, 2022, 108791, ISSN 0360-1323, https://doi.org/10.1016/j.buildenv.2022.108791.
[14] P. Bevilacqua, D. Mazzeo, N. Arcuri, Thermal inertia assessment of an experimental extensive green roof in summer conditions, Building and Environment, Volume 131, 2018, Pages 264-276, ISSN 0360-1323, https://doi.org/10.1016/j.buildenv.2017.11.033.
[15] P. Bevilacqua, D. Mazzeo, M. De Simone, N. Arcuri, A new simulation tool for the evaluation of energy performances of green roofs, Building Simulation Applications BSA, 2015, Pages 313-321, ISBN 978-88-6046-074-5, ISSN 2531-6702. In: Baratieri M; Patuzzi F; Gasparella A; Corrado V, Building simulation applications 2015, Bolzano, Italy, 4-6 Febbraio 2015
[16] L. Cirrincione, M. La Gennusa, G. Peri, G. Rizzo, G. Scaccianoce, S. Aprile, G. Sorrentino, Green roofs as effective tools for improving the indoor comfort levels of buildings-an application to a case study in sicily, Applied Sciences, Volume 10, Issue 3, 893, ISSN 20763417, https://doi.org/10.3390/app10030893.
[17] M. Manso, J. Castro-Gomes, Green wall systems: A review of their characteristics, Renewable and Sustainable Energy Reviews, Volume 41, 2015, Pages 863-871, ISSN 1364-0321, https://doi.org/10.1016/j.rser.2014.07.203.
[18] D. J. Sailor, A green roof model for building energy simulation programs, Energy and Buildings, Volume 40, Issue 8, 2008, Pages 1466-1478, ISSN 0378-7788, https://doi.org/10.1016/j.enbuild.2008.02.001.
[19] S. Frankenstein, G. Koenig, FASST Vegetation Models, U.S. Army Engineer Research and Development Center, Cold Regions Research and Engineering Laboratory (ERDC/CRREL), Technical Report TR-04–25, 2004.
[20] A. D'Amico, G. Ciulla, M. Traverso, V. Lo Brano, E. Palumbo, Artificial Neural Networks to assess energy and environmental performance of buildings: An Italian case study, Journal of Cleaner Production, Volume 239, 2019, 117993, ISSN 0959-6526, https://doi.org/10.1016/j.jclepro.2019.117993.
[21] M. Beccali, G. Ciulla, V. Lo Brano, A. Galatioto, M. Bonomolo, Artificial neural network decision support tool for assessment of the energy performance and the refurbishment actions for the non-residential building stock in Southern Italy, Energy, Volume 137, 2017, Pages 1201-1218, ISSN 0360-5442, https://doi.org/10.1016/j.energy.2017.05.200.
[22] D. Bienvenido-Huertas, J. Moyano, C: E. Rodríguez-Jiménez, D. Marín, Applying an artificial neural network to assess thermal transmittance in walls by means of the thermometric method, Applied Energy, Volumes 233–234, 2019, Pages 1-14, ISSN 0306-2619, https://doi.org/10.1016/j.apenergy.2018.10.052.
[23] N. Premalatha, A. Valan Arasu, Prediction of solar radiation for solar systems by using ANN models with different back propagation algorithms, Journal of Applied Research and Technology, Volume 14, Issue 3, 2016, Pages 206-214, ISSN 1665-6423, https://doi.org/10.1016/j.jart.2016.05.001.

[24] E. F. Alsina, M. Bortolini, M. Gamberi, A. Regattieri, Artificial neural network optimisation for monthly average daily global solar radiation prediction, Energy Conversion and Management, Volume 120, 2016, Pages 320-329, ISSN 0196-8904, https://doi.org/10.1016/j.enconman.2016.04.101.

[25] A. Mellit, M. Benghanem, S.A. Kalogirou, An adaptive wavelet-network model for forecasting daily total solar-radiation, Applied Energy, Volume 83, Issue 7, 2006, Pages 705-722, ISSN 0306-2619, https://doi.org/10.1016/j.apenergy.2005.06.003.

[26] G. Grassi, P. Vecchio, Wind energy prediction using a two-hidden layer neural network, Communications in Nonlinear Science and Numerical Simulation, Volume 15, Issue 9, 2010, Pages 2262-2266, ISSN 1007-5704, https://doi.org/10.1016/j.cnsns.2009.10.005.

[27] A. S. Qureshi, A. Khan, A. Zameer, A. Usman, Wind power prediction using deep neural network based meta regression and transfer learning, Applied Soft Computing, Volume 58, 2017, Pages 742-755, ISSN 1568-4946, https://doi.org/10.1016/j.asoc.2017.05.031.

[28] A.B.G Bahgat, N.H Helwa, G.E Ahamd, E.T El Shenawy, Estimation of the maximum power and normal operating power of a photovoltaic module by neural networks, Renewable Energy, Volume 29, Issue 3, 2004, Pages 443-457, ISSN 0960-1481, https://doi.org/10.1016/S0960-1481(03)00126-5.

[29] D. Mazzeo, M. S. Herdem, N. Matera, M. Bonini, J. Z. Wen, J. Nathwani, G. Oliveti, Artificial intelligence application for the performance prediction of a clean energy community, Energy, Volume 232, 2021, 120999, ISSN 0360-5442, https://doi.org/10.1016/j.energy.2021.120999.

[30] T. Wei, C.Y. Jim, Anqi Chen, X. Li, Adjusting soil parameters to improve green roof winter energy performance based on neural-network modeling, Energy Reports, Volume 6, 2020, Pages 2549-2559, ISSN 2352-4847, https://doi.org/10.1016/j.egyr.2020.09.012.

[31] S.W. Tsang, C.Y. Jim, Applying artificial intelligence modeling to optimize green roof irrigation, Energy and Buildings, Volume 127, 2016, Pages 360-369, ISSN 0378-7788, https://doi.org/10.1016/j.enbuild.2016.06.005.

[32] S. Pandey, D. A. Hindoliya, Ritu mod, Artificial neural network for predation of cooling load reduction using green roof over building in Sustainable City, Sustainable Cities and Society, Volume 3, 2012, Pages 37-45, ISSN 2210-6707, https://doi.org/10.1016/j.scs.2012.01.003.

[33] D. Erdemir, T. Ayata, Prediction of temperature decreasing on a green roof by using artificial neural network, Applied Thermal Engineering, Volume 112, 2017, Pages 1317-1325, ISSN 1359-4311, https://doi.org/10.1016/j.applthermaleng.2016.10.145.

[34] Y. He, E. S. Lin, C. L. Tan, P. Y. Tan, N. H. Wong, Quantitative evaluation of plant evapotranspiration effect for green roof in tropical area: A case study in Singapore, Energy and Buildings, Volume 241, 2021, 110973, ISSN 0378-7788, https://doi.org/10.1016/j.enbuild.2021.110973.

[35] A. Asadi, H. Arefi, H. Fathipoor, Simulation of green roofs and their potential mitigating effects on the urban heat island using an artificial neural network: A case study in Austin, Texas, Advances in Space Research, Volume 66, Issue 8, 2020, Pages 1846-1862, ISSN 0273-1177, https://doi.org/10.1016/j.asr.2020.06.039.

[36] E. M. H. Abdalla, V. Pons, V. Stovin, S. De-Ville, E. Fassman-Beck, K. Alfredsen, T. M. Muthanna, Evaluating different machine learning methods to simulate runoff from extensive green roofs. Hydrology and Earth System Sciences, Volume 25, Issue 11, 2021, Pages 5917-5935, https://doi.org/10.5194/hess-25-5917-2021.

[37] DesignBuilder Software Ltd version 5.5.0, 2019, Website: https://designbuilder.co.uk, accessed on 11 May 2022.

[38] P. Ferrante, M. La Gennusa, G. Peri, G. Scaccianoce, G. Sorrentino, Comparison Between Conventional and Vegetated Roof by Means of a Dynamic Simulation, Energy Procedia, Volume 78, 2015, Pages 2917-2922, ISSN 1876-6102, https://doi.org/10.1016/j.egypro.2015.11.667.

[39] G. Peri, G. Rizzo, G. Gugliuzza, B. Varotta, Design, Building up and First Results of Three Monitored Green Coverings Over a University Department Building, Energy Procedia, Volume 78, 2015, Pages 3037-3042, ISSN 1876-6102, https://doi.org/10.1016/j.egypro.2015.11.719.

[40] L. Cirrincione, M. L. Gennusa, C. Marino, A. Nucara, A. Marvuglia, G. Peri, Passive components for reducing environmental impacts of buildings: analysis of an experimental green roof, 2020 IEEE 20th Mediterranean Electrotechnical Conference (MELECON), 2020, Pages 494-499, https://doi.org/10.1109/MELECON48756.2020.9140546.

[41] P. Ferrante, M. La Gennusa, G. Peri, G. Rizzo, G. Scaccianoce, Vegetation growth parameters and leaf temperature: Experimental results from a six plots green roofs' system, Energy, Volume 115, Part 3, 2016, Pages 1723-1732, ISSN 0360-5442, https://doi.org/10.1016/j.energy.2016.07.085.

[42] Perlite Italiana Srl, Alzaia Trento, Corsico (Milan), Website: http://www.perlite.it/it/edilizia/giardini-pensili/tetto-giardino, accessed on 11 May 2022.

[43] S. Frankenstein, G. Koenig, Fast All-season Soil Strength (FASST), U.S. Army Engineer Research and Development Center, Cold Regions Research and Engineering Laboratory (ERDC/CRREL), Special Report SR-04–01, 2004.

[44] UNI 10351/2015: Materiali da costruzione – Conduttività termica e permeabilità al vapore ("UNI 10351/2015: Building Materials - Thermal Conductivity and Vapor Permeability") in Italian.

[45] UNI 10355/2013: Murature e solai – Valori della resistenza termica e metodo di calcolo ("UNI 10355/2013: Walls and floors - Thermal resistance values and calculation method") in Italian.

[46] UNI EN 1745/2012: Murature, solai, malte e intonaci ("UNI EN 1745/2012: Walls, floors, mortars and plasters") in Italian.

[47] UNI EN ISO 10456/2008: Materiali e prodotti per edilizia - Proprietà igrometriche - Valori tabulati di progetto ("UNI EN ISO 10456/2008: Building Materials and Products - Hygrometric Properties - Tabulated Design Values") in Italian.

[48] UNI/TR 11552/2014: Abaco delle strutture costituenti l'involucro opaco degli edifici – Parametri termofisici ("UNI/TR 11552/2014: Abacus of the structures constituting the opaque envelope of buildings - Thermophysical parameters") in Italian.

[49] DesignBuilder Software Ltd version 5.5.0, 2019. Website: https://designbuilder.co.uk/helpv3.0/Content/GreenRoof.htm, accessed on 11 May 2022

[50] M. Mahmoodzadeh, P. Mukhopadhyaya, C. Valeo, Effects of Extensive Green Roofs on Energy Performance of School Buildings in Four North American Climates, Water, Volume 12, Issue 1, 2020, 6; https://doi.org/10.3390/w12010006.

[51] D. J. Sailor, D. Hutchinson, L. Bokovoy, Thermal property measurements for ecoroof soils common in the western U.S., Energy and Buildings, Volume 40, Issue 7, 2008, Pages 1246-1251, ISSN 0378-7788, https://doi.org/10.1016/j.enbuild.2007.11.004.

[52] P. Kim, Matlab deep learning, With Machine Learning, Neural Networks and Artificial Intelligence, Volume 130, Issue 21, 2017, eBook ISBN 978-1-4842-2845-6, https://doi.org/10.1007/978-1-4842-2845-6

[53] Levenberg-Marquardt backpropagation, Deep Learning Toolbox, ©COPYRIGHT 1992-2004 by The MathWorks, Inc. Natick, Massachusetts, United State. Website: https://www.mathworks.com/help/deeplearning/ref/trainlm.html.

[54] M. T. Hagan, H.B. Demuth, M.H. Beale, Neural network design, PWS Publishing, Boston, MA, 1996.

[55] M. T. Hagan, M.B. Menhaj, Training feedforward networks with the Marquardt algorithm, IEEE Trans Neural Network, Volume 5, Issue 6, 1994, Pages 989-993, https://doi.org/10.1109/72.329697, ISSN 1941-0093.

[56] Neural net fitting tool, Deep Learning Toolbox, ©COPYRIGHT 1992-2004 by The MathWorks, Inc. Natick, Massachusetts, United State, Website: https://www.mathworks.com/help/deeplearning/ref/nftool.html, accessed on 11 May 2022.

[57] A. H. Elsheikh, S. W. Sharshir, M. A. Elaziz, A.E. Kabeel, W. Guilan, Z. Haiou, Modeling of solar energy systems using artificial neural network: A comprehensive review, Solar Energy, Volume 180, 2019, Pages 622-639, ISSN 0038-092X, https://doi.org/10.1016/j.solener.2019.01.037.

Declaration of interest Statement

Authors' names: Domenico Mazzeo[1,*], Nicoletta Matera[2], Giorgia Peri[3], Gianluca Scaccianoce[3]

[1]Department of Mechanical, Energy and Management Engineering (DIMEG), University of Calabria, Rende (CS), 87036, Italy
[2]Indipendent researcher, Rende (CS), 87036, Italy
[3]Department of Engineering, University of Palermo, Palermo, 90128, Italy

Title of article: Forecasting green roofs' potential in improving building thermal performance and mitigating urban heat island in the Mediterranean area: an artificial intelligence-based approach

Signature: 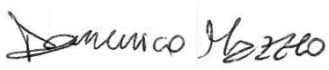

Date: 27/06/2022

x I have no relevant interest(s) to disclose.
□ I have potentially relevant interest(s) as outlined below (if more space is required, please document the information in an attachment):

_____

Credit Author Statement

DM: Conceptualization, Methodology, Software, Validation, Formal analysis, Investigation, Resources, Data Curation, Writing - Original Draft, Writing - Review & Editing, Visualization

NM: Methodology, Software, Validation, Formal analysis, Data Curation, Writing - Review & Editing, Visualization

GP: Formal analysis, Investigation, Resources, Writing - Original Draft, Writing - Review & Editing, Visualization

GS: Investigation, Resources, Writing - Review & Editing, Visualization